upna

ISC
Institute of
Smart Cities

SMART CITIES: Future trends and challenges 2021

- Smart environments
- Sustainability and energy efficiency
- Data analysis and signal processing
- Internet of things

Introduction

The session “Smart Cities: Future trends and challenges - 2021” was held the 17 of December of 2021 in the Public University of Navarre. Its main objective was to convey to the future researchers of the ISC the importance of conducting international research. This was done by inviting renowned experts with international experience as well as holding a poster presentation in English.

The experts were:

- Jesse de Pelegrin - “Development of Optical Instrumentation Techniques Applied in Electrical Machines” - Professor Federal Institute Catarinense, Brazil
- Dr. Rafael Morales - “Emerging technologies on novel interactive systems” - Haptic Engineer at Ultraleap Ltd.
- Dr. Bartosz Sawik - “Multi-Criteria Optimizations in Logistics and Supply Chains” - Haas School of Business, University of California at Berkeley
- Dr. Iñigo Garbayo - “Round trip to your hometown: Building a career in Energy materials” - CENER, Manager of Hydrogen Area

The Institute of Smart Cities (ISC) is a R&D institute of the Public University of Navarra (UPNA), its purpose is to lead the development of technology and services for Smart Cities. Smart Cities combine sensors, networks, data processing, energy storage and user interfaces to control electricity, traffic, water, waste, citizen engagement and other aspects in an efficient and integrated way.

The ISC is formed by 15 Principal investigators, 54 Senior Researchers, 35 Postdoctoral researchers, 7 Postdoctoral Trainees and 12 Predoctoral Trainees. Our researchers are classified into 4 main research lines: “Smart environments & Wellbeing”, “Sustainability and energy efficiency”, “Data analysis and signal processing” and “Communications, Sensors & IoT”.

Urban spaces are experiencing a radical transformation that will deeply impact the way we live, move and interact with other people and infrastructures. To face this transformation, the transverse nature of the ISC is of paramount importance. ISC research covers everything from the development of new quantum sensors, to the evaluation of deployed systems in a real city. Our multidisciplinarity allows us to cover both the technical aspects and the policy making, with the end-goal of improving life quality and sustainability inside cities and smart environments.

The ISC is oriented towards achieving international excellence in R&D, it is also committed to the economic, social and sustainable development of Navarra, with a deep imbrication with public and private institutions of the region.

Experimental development of a novel thermoelectric generator without moving parts to harness shallow hot dry rock fields

Patricia Alegria
Department of Engineering,
Institute of Smart Cities,
Public University of Navarre,
Pamplona, Spain
patricia.alegria@unavarra.es

Antonio Rodriguez
Department of Engineering,
Institute of Smart Cities,
Public University of Navarre,
Pamplona, Spain
antonio.rodriguez@unavarra.es

Leyre Catalan
Department of Engineering,
Institute of Smart Cities,
Public University of Navarre,
Pamplona, Spain
leyre.catalan@unavarra.es

David Astrain
Department of Engineering,
Institute of Smart Cities,
Public University of Navarre,
Pamplona, Spain
david.astrain@unavarra.es

Miguel Araiz
Department of Engineering,
Institute of Smart Cities,
Public University of Navarre,
Pamplona, Spain
miguel.araiz@unavarra.es

***Abstract*—Nowadays, geothermal energy in shallow hot dry rocks is not exploited enough due to the high economic and environmental impact as well as the lack of scalability of the existing technologies. Here, thermoelectricity has a great future potential due to its robustness, absence of moving parts and modularity. With this research, the feasibility of a novel and robust geothermal thermoelectric generator whose working principle is phase change has been experimentally demonstrated, as well as the importance of compactness to maximize its efficiency and thus, power generation.**

Keywords—Thermoelectric generator, Heat pipe, Thermosiphon, Fins dissipator, Thermoelectricity.

I. Introduction

Nowadays, the only existing technologies to convert geothermal energy into electricity are geothermal power plants, which are only profitable for elevated powers. Timanfaya National Park is the biggest hot dry rock field, where temperatures up to 400 ºC can be found at 1m deep inside the ground [1]. The existing method to harness this kind of fields is Enhanced Geothermal System, which requires fracturing the rock and may cause seismicities [2]. The elevated environmental and visual impact, as well as the lack of scalability make it impossible to implement this method in Timanfaya. Here, thermoelectricity has a great future potential. A geothermal thermoelectric generator is a solid-state device that directly transforms thermal energy from the superficial Earth's crust into usable electricity, it is very compact, without moving parts and it causes a low environmental impact. It contains three principal parts: The hot side heat exchanger (HHE), the thermoelectric module (TEM) and the cold side heat exchanger (CHE). The hot side heat exchanger transports the heat from a heat source (the geothermal source) to the hot side of the TEM.

The thermoelectric module is the most important part, which is responsible of transforming part of the heat into electricity thanks to the Seebeck effect. The heat that is not transformed into electric energy must be dissipated into the cold source, usually the environment, for which a CHE is used. The module's efficiency highly depends on the temperature difference between its hot and cold sides.

Different thermoelectric generators (TEG) for geothermal energy can be found in the literature. Most are computational studies and few experimental, and what is more, in order to apply thermoelectric generation to geothermal energy, all of them use moving parts to circulate a fluid [3], thus losing the intrinsic advantage of thermoelectricity: the absence of moving parts.

The only TEG proposed to take advantage of the high enthalpy geothermal anomalies in hot dry rock fields is the one designed, computationally studied by Catalan et al. [4]. It consists of biphasic thermosiphons with water as working fluid in both sides of the thermoelectric modules. As laboratory and field work should be done, this research deepens in the experimental operation of a geothermal thermoelectric generator based on biphasic passive heat exchangers, with the objective of obtaining the maximum power generation and optimizing the occupied space. Furthermore, the objective is to demonstrate the viability of this kind of devices to harness shallow hot dry rock fields.

In Section 2, the heat exchangers are experimentally studied to select the best option for both the hot and cold sides. In Section 3, the results of the GTEG's experimentation are collected and finally, Section 4 contains the conclusions of the work.

II. Characterization of the Heat Exchangers

A. Hot side heat exchanger

The hot side heat exchanger is a biphasic closed thermosiphon with water as working fluid, which was characterized by applying a heat flux through its lower part and determining the temperature drop from the bottom to the top. Its thermal resistance was also calculated according to (1), by measuring its surface temperature, the ambient temperature and the heat flux passing.

$$R_{th} = \frac{T_{surf} - T_{amb}}{\dot{Q}} \quad (1)$$

The maximum temperature drop was from 160 ºC to 145 ºC, with a thermal resistance of 0.07 K/W for a 160 W heat flux, which shows the good performance of this heat exchanger.

B. *Cold side heat exchanger*

The cold side heat exchanger consists of four 500 mm long sintered heat pipes with a diameter of 8 mm inserted horizontally and then inclined in a 70×90mm^2 fins dissipater with a base 14.5 mm thick and fifteen 40×1.5mm^2 corrugated fins.

It was characterized with the same method in order to select the most effective geometry, which permits more compactness so that the visual impact is minimum. The result of the characterization was a thermal resistance value of 0.4 K/W, constant with the heat flux.

III. Generation Results

O nce proved that both the hot and cold side heat exchangers have low thermal resistance values and are appropriate for the geothermal thermoelectric generator, the complete generator was built. It was decided to build two prototypes, one with 10 modules and other with 6, in order to compare if the addition of thermoelectric modules increases the output power.

The generator was experimented in laboratory during 10 days under different hot source temperature and external convection conditions. Temperatures and power generation were measured as shown in Figure 1. The total generated power was of 36 W (17 W by a prototype with 10 modules and 19 W by a prototype with 6 modules) for a temperature difference of 160ºC between the heat source and the environment. The efficiency diminished from 4.06% in the prototype with 6 modules to 3.72% in the one with 10, showing the importance of compactness in these generators.

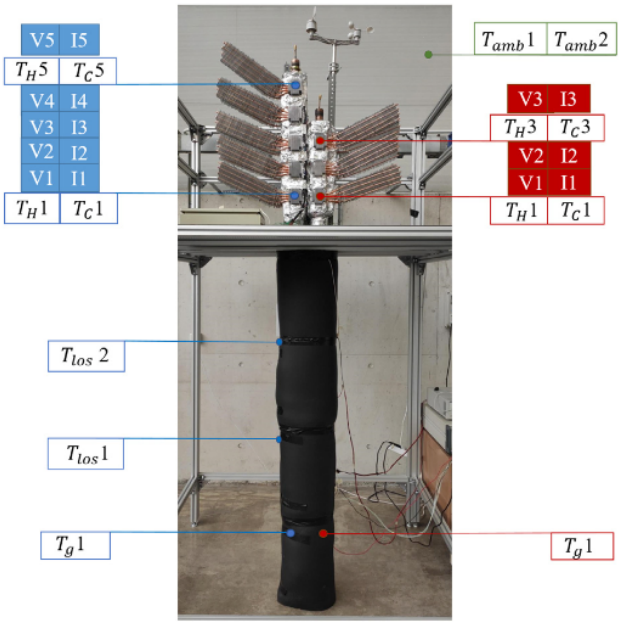

Figure 1. Complete prototype with measuring points in laboratory tests.

IV. Conclusions

In conclusion, this research has demonstrated experimentally the feasibility of thermoelectricity to generate electricity from high enthalpy geothermal anomalies in shallow hot dry rock fields. The generator developed in this work is capable of generating 36 W in total with a temperature difference between the heat source and the environment of 160ºC, without auxiliary consumption. In short, a passive generator that demonstrates the viability of this technology to take advantage of the natural resources as high enthalpy geothermal anomalies present in shallow hot dry rock fields and to provide electricity in a renewable and environmentally friendly way.

References

[1] G. Camacho, J.F. Prieto, E. Ancochea, J. Fernández, Deep volcanic morphologybelow Lanzarote, Canaries, from gravity inversion: New results for Timanfaya andimplications, J. Volcanol. Geotherm. Res. 369 (2019) 64–79, http://dx.doi.org/10.1016/j.jvolgeores.2018.11.013.

[2] W. Brown, D.V. Duchane, G. Heiken, V.T. Hriscu, Mining the Earth's Heat:Hot Dry Rock Geothermal Energy, Springer-Verlag Berlin Heidelberg, 2012,http://dx.doi.org/10.1007/978-3-540-68910-2, URL https://www.springer.com/gp/book/9783540673163

[3] R. Takleh, V. Zare, Employing thermoelectric generator and booster com-pressor for performance improvement of a geothermal driven combined powerand ejector-refrigeration cycle, Energy Convers. Manage. 186 (2019) 120–130, http://dx.doi.org/10.1016/j.enconman.2019.02.047.

[4] L. Catalan, M. Araiz, P. Aranguren, D. Astrain, Computational study ofgeothermal thermoelectric generators with phase change heat exchangers, En-ergy Convers. Manage. 221 (2020) http://dx.doi.org/10.1016/j.enconman.2020.113120.

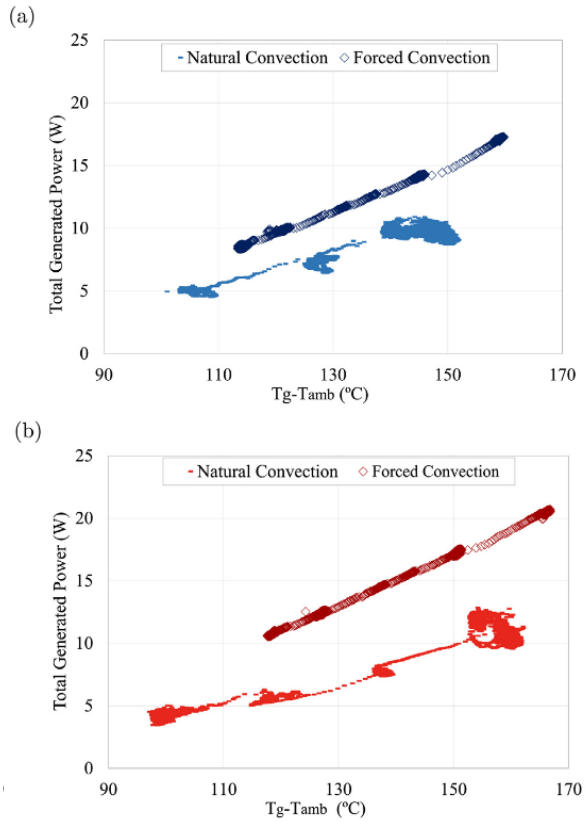

Figure 2. a) Total generated power by Prototype with 10 modules. b) Total generated power by Prototype with 6 modules.

Virtual reality environments for cognitive and motor rehabilitation

Yaiza Álvarez
PhD Student
Dept. of Statistics, Computer Science and Mathematics
Public University of Navarre
Pamplona, Spain
yaiza.alvarez@unavarra.es

Jose Javier Astrain
Dept. of Statistics, Computer Science and Mathematics
Public University of Navarre
Pamplona, Spain
josej.astrain@unavarra.es

***Abstract*—Virtual reality (VR) consists of the sensory immersion of the user in an artificially generated environment. Head mounted Displays (HMDs) are usually used to introduce the user into these VR environments. Although the most common use of VR is more focused on video games, it has been also researched for its use in learning environments, focusing on cognitive and functional rehabilitation. The benefit of this is that multiple customizable environments or situations can be created, without the limitations of real physical scenarios. Real-life situations can be simulated, helping the user to enhance learning and skill development to everyday circumstances, without the risks or resources present in real life circumstances.**

***Keywords*—virtual reality (VR), rehabilitation, intellectual disabilities, physical disabilities.**

I. Introduction

Virtual reality (VR) is a set of digital computer-generated scenes able to simulate real environments. VR generates in the user the sensation of immersion in these virtual environments. These scenarios can be provided to the user through devices known as virtual reality glasses or headsets.

Stereoscopic Head-mounted Displays consist of two screens on which the user can see a different video sequence in each eye. By means of stereoscopic vision, the user perceives it as a three-dimensional space. VR environments do also enhance dynamic and interactive perception. In addition, the glasses include inertial and positioning sensors to be able to react to the movements made by the user and thus offer an immersive interactive experience. Therefore, when the user walks or moves his head or hands in the real world, his virtual avatar also does so in the virtual world.

II. Examples Of Virtual Reality In Rehabilitation

Virtual Reality is an innovative and promising technology for motor and cognitive rehabilitation. Wu, T. proposes a study analyzing the usability of an easy-to-use adaptation of the ”Virtual Reality Vocational Skills Training System” in high school students with intellectual disabilities [1]. Two differences between the original and easy-to-use versions were reported: added voice prompts and simplified the control buttons. Eight students with intellectual disabilities were chosen to participate in the study. The results were very positive, indicating that the easy-to-use version had good usability. The students were able to reduce the operation time and the number of wrong actions, as well, their accuracy was enhanced.

Brooks, B. evaluates the efficiency of using a virtual kitchen for vocational training of people with intellectual disabilities [2]. The results showed that virtual learning was as beneficial as real physical learning and that it was also better than learning through a book. The users were able to use the virtual kitchen environment and were motivated to learn with this training method.

Apart from learning, VR can be applied for functional rehabilitation. Pereira, M. propose a VR game to improve hand rehabilitation [3]. It evaluates the usability of the Oculus Quest for participants undergoing functional rehabilitation. Results were very favorable in terms of usability.

Choi, J. published an article in which VR games were used to promote wrist and forearm joint movements [4]. The results displayed significant improvements in upper extremity dexterity functions, in the performance of activities of daily living, and in forearm supination by kinematic analysis.

Mathews, M. developed a therapy that consisted of teaching users memory techniques using a computer [5]. Then, they practiced them in VR environments. This allowed the user’s actions to be recorded and individual instant feedback to be provided to the user. The final results indicated that this therapy was very effective.

III. Methodology

In order to define the working methodology of the PhD, the Brainsens collaborative research project (Fig. 1) has been taken as a reference. This project has been carried out at the Public University of Navarre by Álvarez, Y.

A. Participants

An important aspect of the project is user testing. To gather enough user data, it will be required to contact centers or institutions that might be interested in physical and cognitive rehabilitation. At least two kinds of user groups will be studied. Users with functional disabilities as ictus or strokes, and cognitive impairment as down syndrome or intellectual disabilities.

Figure 1. Brainsens project: kitchen and supermarket environment.

B. *Devices*

Priorly, a study will be made to choose the most suitable VR devices for carrying out the exercises. This decision will be made based on the usability and immersion capabilities of the HMD.

C. *Environment design*

Once the right device has been chosen and there is a clear understanding of how the environments and exercises will be structured, the development stage of the VR system will begin.

Figure 2. An example of VR scenario from the Brainsens project.

The proposal is to set up exercises using hand controls and to study the potential application of hand tracking. This is a technique in which the user's hands are the controls used to interact with the environment. However, it is something that is still under development, although simple exercises focused more on functional rehabilitation could be proposed. In order to collect useful user feedback, user testing about usability and subjective perceived workload will be carried out to check the implemented functions, so problems can be detected quickly and readjustments can be made in time.

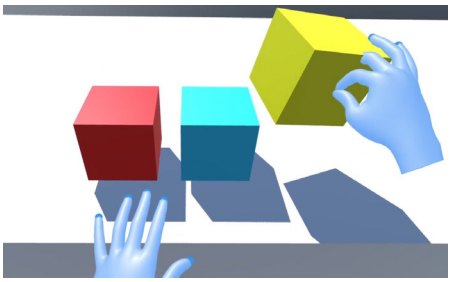

Figure 3. An example of VR scenario with hand tracking.

D. *Data collecting*

During the development of the exercises, the data that the healthcare workers or social-health workers consider necessary

will be collected. These data will be evaluation parameters to analyze if the patient is progressing favorably or not. Thanks to the wifi connection that the virtual reality devices have, the data collected could be sent to a specific application, allowing analyzing the results obtained for each exercise.

IV. Discussion

Technological advances in the area of virtual reality open up new possibilities in the development of applications in the health sector. From the rehabilitation approach, virtual reality provides the opportunity to practice activities that are not, or cannot be, practiced in a clinical setting. In addition, virtual reality environments can be designed to be more interesting and visually appealing than traditional therapy techniques, thus encouraging user participation and repetitiveness, which can lead to better progress [6].

V. Future work

The proposal of this PhD is to develop a software tool that allows virtual rehabilitation exercises to be performed independently of the limitations of the real environment. The only requirements would be: to have a VR device with which to do the exercises and to adapt the environment of the session to the activity (e.g.: clear the room, or define constraints as the users being seated, having a table in front of they or not, etc.).

The challenge posed in this PhD is to improve the most important cognitive and physical functions in patients undergoing rehabilitation, such as attention, orientation, memory, motor functions, and visuospatial skills (ability to represent, analyze and manipulate objects mentally).

This project is intended not only to help patients with some kind of disability but also to help those who are responsible for the rehabilitation sessions, providing them a software tool with scenarios or exercises that, due to the limitations of the installations or the center, cannot be carried out.

Acknowledgment

The Brainsens (0011-1365-2019-000076) research was funded by the Government of Navarre and the European Union with FEDER funds.

References

[1] Wu, T. (2020) "Usability of Virtual Reality Vocational Skills Training System for Students with Intellectual Disabilities", International Conference on Computers Helping People with Special Needs, pp. 123-129, Springer, Cham.

[2] Brooks, B (2002) "An evaluation of the efficacy of training people with learning disabilities in a virtual environment", Disabil. Rehabil., vol. 24, no. 11-12, pp. 627-633.

[3] Pereira, M. (2020) "A Virtual Reality Serious Game for Hand Rehabilitation Therapy", 2020 IEEE 8th Int. Conf. Serious Games Appl. Heal. SeGAH.

[4] Choi, J. (2021) "Virtual reality rehabilitation in children with brain injury: a randomized controlled trial", Dev. Med. Child Neurol., vol. 63, no. 4, pp. 480-487.

[5] Mathews, M. (2016) "A Virtual Reality Environment for Rehabilitation of Prospective Memory in Stroke Patients", Procedia Comput. Sci., vol. 96, pp. 7-15.

[6] Laver, K. (2012) "Virtual reality for stroke rehabilitation", Stroke, vol. 43, no. 2, pp. 20-21.

PhantomFields: Fast Time and Spatial Multiplexation of Acoustic Fields for Generation of Superresolution Patterns

Sonia Elizondo Martínez
UpnaLab
Universidad Pública de Navarra
Pamplona, Navarre, Spain
sonia.elizondo@unavarra.es

Jaime Goñi
UpnaLab
Universidad Pública de Navarra
Pamplona, Navarre, Spain
jaimegonicarnicero@hotmail.com

Mikel Galar Idoate
Departamento de Estadística, Informática y Matemáticas
Universidad Pública de Navarra
Pamplona, Navarre, Spain
mikel.galar@unavarra.es

Asier Marzo Pérez
UpnaLab
Universidad Pública de Navarra
Pamplona, Navarre, Spain
asier.marzo@unavarra.es

***Abstract*—Ultrasonic fields generated by phased arrays can be tailored to obtain a custom pattern of acoustic radiation forces. These force fields can pattern particles as well as be felt by the human hand, enabling applications for bioprinting and contactless haptic devices. The force fields can be switched orders of magnitude faster than the reaction time of the particles that it pushes or the human mechanoreceptors of touch. Therefore, a quick multiplexation in time or in space of different acoustic fields will be perceived as the average field. In this paper, we optimise the non-linear problem of decomposing a target force field into several multiplexed acoustic fields. We create averaged fields, PhantomFields, that cannot be created by a regular (unique) emission of an acoustic field. We improve accuracy by time multiplexation and spatial multiplexation, i.e. quick rotation of the emitters. These processes improve the resolution and strength of the obtained fields without the requirement of new hardware, opening up applications in haptic devices and 3D printing.**

***Keywords*—acoustic fields, phased-arrays, multiplexation**

I. Methods and apparatus

Phased arrays are used to generate ultrasonic fields. These arrays are composed of a certain number of acoustic transducers arranged as different geometrical shapes. For this work, a square array and a radial array have been used (Fig. 1). They have 1cm diameter ultrasonic emitters operating at 40 kHz.

The shapes and the limited number of transducers of these phased arrays lead to inaccuracies in the generated acoustic patterns when emitting a single field. To achieve higher resolution patterns without the need of new hardware, we introduce a different technique for their creation: the use of time and spatial multiplexation (Fig. 2). The multiplexation technique consists on creating various partial patterns and switch between them fast enough to achieve an improved average field in terms of resolution and strength. In the case of time-multiplexation, this combination is done in a reduced period of time, emitting one partial field in each instant. The spatial-multiplexation relies on the quick rotation of the phased array, creating one decomposed field for each array position.

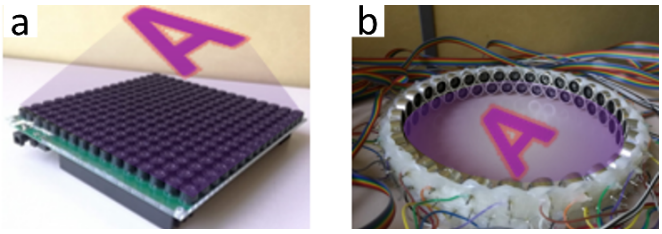

Figure 1. Phased Arrays: a) Square array of 16 × 16 transducers. b) Radial array of 64 transducers and 12cm radius.

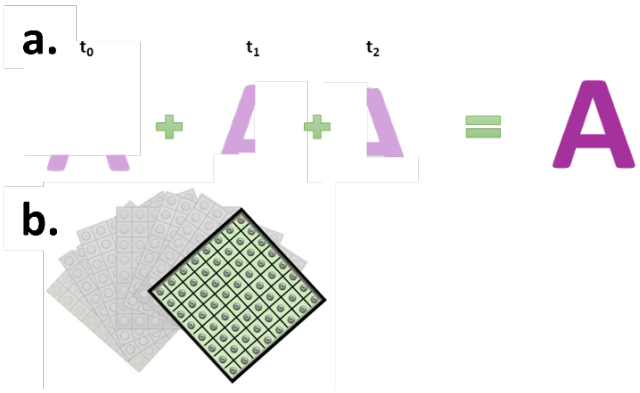

Figure 2. Multiplexing: a) Example of a pattern created by the time multiplexation technique. b) Example of the movement of the array for the spatial multiplexation technique.

II. Applications

Acoustic patterns can be benefitial for several applications, such as the manipulation of small objects (Fig. 3) and the creation of patterns of different matter (Fig. 4). Also, it opens up new opportunities for bioprinting and haptic devices, due to its relation with the tactile perception of acoustic patterns in the human skin.

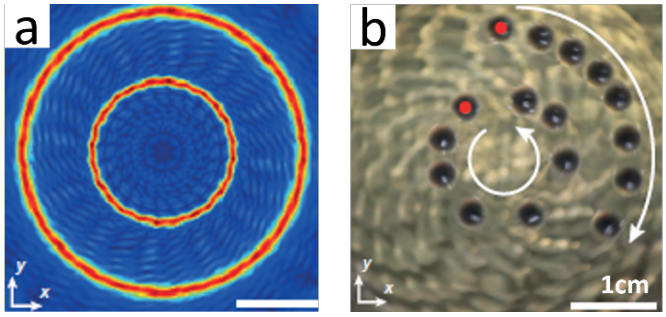

Figure 3. Manipulation of particles by acoustic fields [1]: a) Acoustic field amplitude. b) Two particles being moved by the acoustic field.

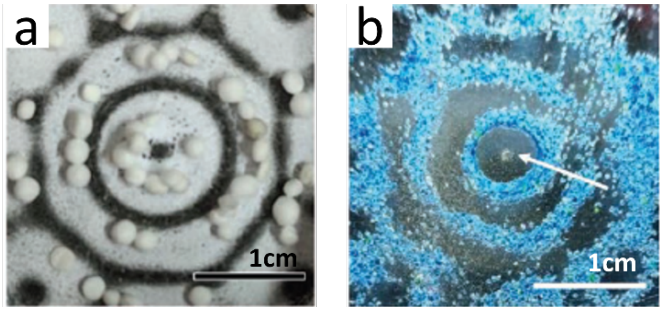

Figure. 4. Particle patterning [2]: a) Carbon-based conductive ink and polystyrene beads on paper. b) Sand and smaller dust fragments.

III. Main results

To optimise the non-linear problem of decomposing a target force field into several multiplexed acoustic fields, various simulations have been carried out. MATLAB has been selected as the engine to proceed with this optimizations and simulations. Various target patterns have been used, such as the ones shown in Fig. 5.

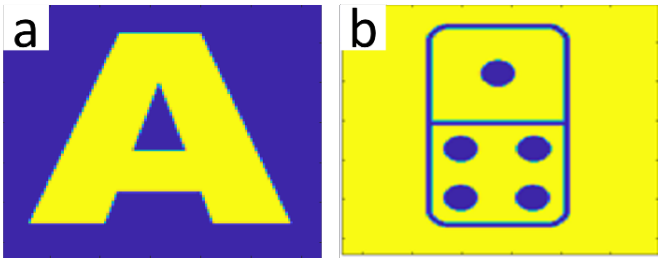

Figure 5. Example of patterns: a) 'A' and b) 'domino'.

In Figures 6 and 7, main results for two different patterns are shown. These patterns have $10cm \times 10cm$ in size. In both cases 16 multiplexations have been considered, which means that the resulting average field is composed of 16 multiplexed acoustic fields. For the 'A' pattern, a square array of 8×8 transducers has been simulated and, in the case of the 'domino' pattern, a radial array with a 12cm radius composed of 64 emitters.

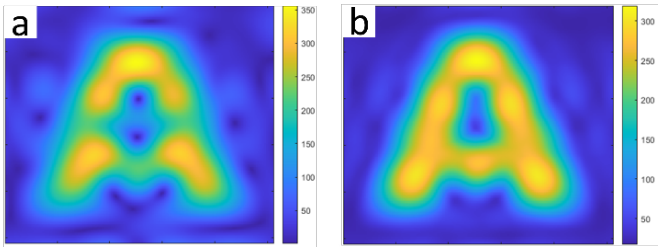

Figure. 6. Pattern 'A': comparison between a) unique emission and b) 16 multiplexed fields.

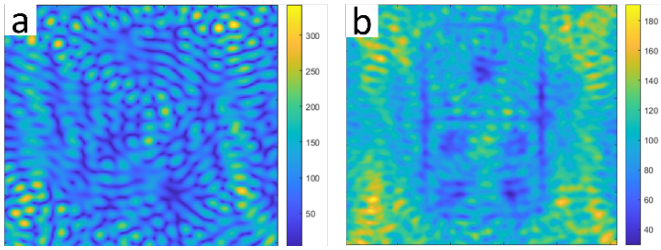

Figure 7. Pattern 'domino': comparison between a) unique emission and b) 16 multiplexed fields.

IV. Future work

In following steps, due to the promising simulated results, an experimental setup will be configured. In this way, the viability of the multiplexation techniques can be tested in a real environment, for instance, creating patterns on an oil bath.

Acknowledgment

This project has received funding from the EU Horizon 2020 research and innovation programme under grant agreement No 101017746.

References

[1] K. Melde, A. G. Mark, T. Qiu and P. Fischer, "Holograms for acoustics", Nature, vol. 537, no 7621, p. 518-522, 2016.

[2] J. Shapiro, B.W. Drinkwater, A.W. Perriman and M. Fraser, "Sonolithography: In-Air Ultrasonic Particulate and Droplet Manipulation for Multiscale Surface Patterning", Advanced Materials Technologies, vol. 6, no 3, p. 2000689, 2021.

Experimental study of a multistage thermoelectric heat pump using different internal heat exchangers

Irantzu Erro
Department of Engineering
Public University of Navarre
Pamplona, Spain
irantzu.erro@unavarra.es

Patricia Aranguren
Department of Engineering, Institute of Smart Cities
Public University of Navarre
Pamplona, Spain
patricia.arangureng@unavarra.es

David Astrain
Department of Engineering, Institute of Smart Cities
Public University of Navarre
Pamplona, Spain
david.astrain@unavarra.es

***Abstract*— The current need to carry out an energy transition towards a 100 % renewable horizon places the energy storage as the key. Thermal energy storage has the potential to be an optimal technology. Nowadays electrical resistors are used to convert electrical energy to thermal energy by heating an air flux which is stored afterwards. In this work, it is proposed to use a multistage thermoelectric heat pump (MS-TEHP) to do this energy conversion. It has been experimentally analyzed and compared the performance of two MS-TEHP with different internal heat exchangers. With this preliminary research, it has been demonstrated the feasibility of this novel thermoelectric technology which aim is to improve the energy conversion process for thermal energy storage.**

Keywords—Thermoelectric heat-pump, Multistage, Heat exchanger, Thermoelectricity

I. Introduction

Nowadays, the energy storage is the only way to slow down the climate change, being able to solve the natural intermittency of renewable energies. Thermal energy storage has a great potential to keep exceeding renewable energy. Currently, electrical resistors are used to transform the exceeding electrical energy to thermal energy by heating an air flux, obtaining a coefficient of performance (COP) of one. Then this heated air flux is kept together with solid refractory material as thermal energy in a tank. Therefore, it is possible to store renewable energy when it is required.

In order to improve energy conversion, it is proposed to use thermoelectric modules (TEMs) working as heat pumps for heating the air flux. A TEM is able to transform electrical energy into thermal energy with greater coefficients of performance, COPs, than one, values that depend on working conditions. Principally they depend on reservoirs temperature. The dissipated heat to the hot reservoir is the sum of the absorbed heat from the cold reservoir and the consumed power, as it is shown in Fig. 1. Diaz de Garayo et al. [1] demonstrated the higher the difference between hot and cold reservoirs temperatures, the worse the COP of a TEM is. In this case, considering hot reservoir temperature the same as the thermal energy storage, which usually is between 373 K and 1273 K, and the cold reservoir temperature being the ambient or an industrial heat waste temperature, that is normally around 298 K and 333 K, the temperature difference between reservoirs is considerable.

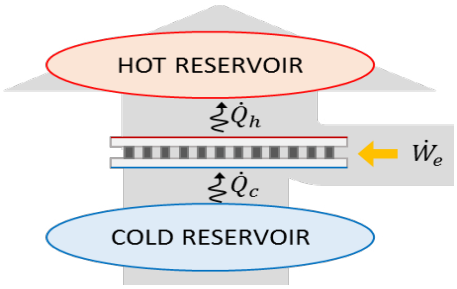

Figure 1. Thermoelectric module (TEM) working as a heat pump.

To make TEMs operate between a lower temperature difference, a novel multistage thermoelectric heat pump (MS-TEHP) is developed. This technology presents many advantages: scalability, minimum maintenance, no refrigerants, reliability, easiness of control and no moving parts.

In this research, there are designed two types of MS-TEHPs, which main difference is the internal heat exchanger (INT-HX) between stages. The first INT-HX is based on a conventional aluminium block, while the second one is a novel heat exchanger based on phase change. So as to accurately study the influence of these internal heat exchangers on the MS-TEHP performance, in this work there are studied two-stage thermoelectric heat pumps heating an air flux. The designs consist of 1 TEM in the 1st stage and 2 TEMs in the 2nd stage, thermally connected by designed INT-HXs. Finally, a finned heatsink is used in the role of heat absorber and commercial heat pipe are selected, due to the good performance studied by Aranguren et al. [2]

II. Characterization of Internal Heat Exchangers

A test bench has been built to characterize the thermal resistance (R_{th}) of the internal heat exchangers (INT-HXs), which is illustrated by Fig. 2.

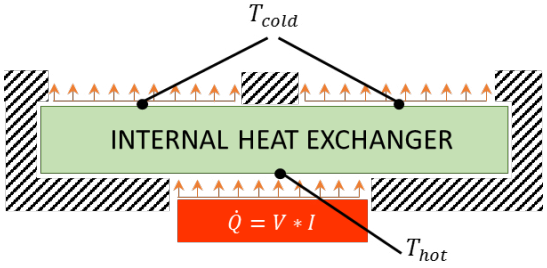

Figure 2. Internal heat exchanger characterization test bench.

The R_{th} has been calculated by (1) for different heat flux supplies on the 1st stage side, measuring the temperature drop between stages.

$$(1)\quad R_{th} = \frac{T_{hot} - T_{cold}}{\dot{Q}}$$

Fig.1 shows the calculated thermal resistance variation in function of the heat flux supply. In case of the 1st INT-HX the thermal resistance (R_{th},1) is almost constant at 0,15 K/W, presenting no heat flux dependence. Meanwhile, the 2nd INT-HX thermal resistance (R_{th},2) suffers a decrease when heat flux supply increases, reaching a value of 0,07 K/W, being this thermal resistance a 50 % lower thermal resistance.

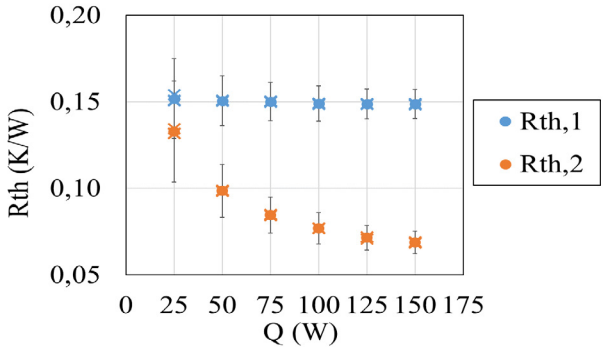

Figure 3. Thermal resistance calculated by (1) for heat exchangers based on conduction and phase change effect (Rth,1 and Rth,2) with different heat flux supply (25, 50, 75, 100, 125 and 150 W)

III. Multistage thermoelectric heat pump analysis

Once the two INT-HXs have been characterized, two MS-TEHP prototypes have been built and tested. Each prototype consists of three MS-TEHPs with different INT-HX in series for heating an air flux, as Fig. 4 presents.

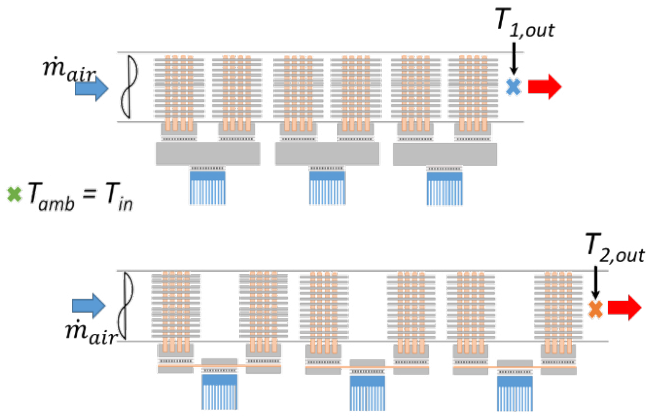

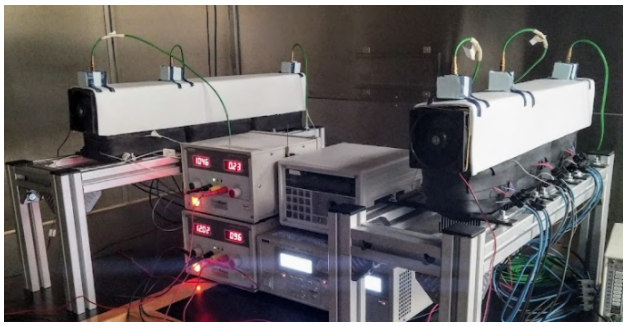

Figure 4. Multistage thermoelectric heat pump prototypes test bench.

It has been experimentally analyzed and compared the performance of two MS-TEHP with different internal heat exchangers. It has been tested both prototypes for different voltage supplies with 25 °C as ambient temperature and an air flow of 45 m³/h. All TEMs are operated at the same voltage in each tested configuration. Fig. 5 shows measured outlet temperature for both prototypes while Fig. 6 represent calculated COP using expression (2).

$$(2)\quad COP = \frac{\dot{Q}_{h,i}}{\dot{W}_{e,i}} = \frac{(\dot{m}_{air} c_p)(T_{out,i} - T_{in})}{V_i \cdot I_i}$$

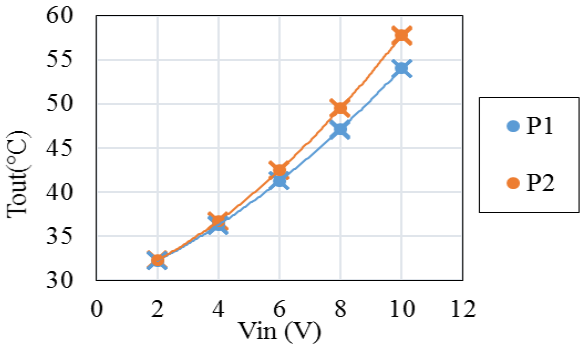

Figure 5. Outlet Temperature for different voltage supply (2, 4, 6, 8 and 10V).

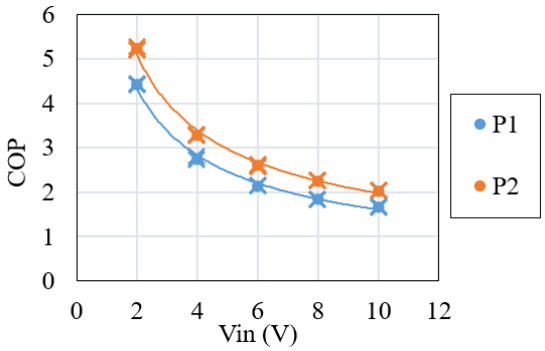

Figure 6. Calculated COP for different voltage supplies (2, 4, 6, 8 and 10V) in each prototype.

Temperature measurements demonstrate the higher the supply voltage, the higher the outlet temperature is. It has been obtained more than 30 °C temperature increase at 10 V supply. Regarding the prototypes operating performance, both prototypes achieve greater COPs than 1,5 for all voltage supplies, having a maximum value of 5. Furthermore, the prototype with phase change INT-HX always shows a 20 % increase in terms of COP.

IV. Conclusions

In this research, it has been designed, built and tested a novel multistage thermoelectric heat pump with different configurations. The possibility of using thermoelectric technology in order to improve energy conversion in thermal energy storage process has been demonstrated.

References

[1] S. Diaz de Garayo, A. Martínez, P. Aranguren, and D. Astrain, "Prototype of an air to air thermoelectric heat pump integrated with a double flux mechanical ventilation system for passive houses," *Appl. Therm. Eng.*, vol. 190, no. October 2020, p. 116801, 2021, doi: 10.1016/j.applthermaleng.2021.116801.

[2] P. Aranguren, S. DiazDeGarayo, A. Martínez, M. Araiz, and D. Astrain, "Heat pipes thermal performance for a reversible thermoelectric cooler-heat pump for a nZEB," *Energy Build.*, vol. 187, pp. 163-172, 2019, doi: 10.1016/j.enbuild.2019.01.039.

LeviPrint: Contactless Additive Manufacturing using Acoustic Levitation with Position and Orientation Control of Elongated Parts

Íñigo Fermín Ezcurdia Aguirre
UpnaLab
Public University of Navarre
Pamplona, Spain
inigofermin.ezcurdia@unavarra.es
https://orcid.org/0000-0003-4268-6760

Rafael Morales González
Ultraleap Ltd.
Bristol BS2 0EL, UK
rafael.morales@ultraleap.com

Asier Marzo Pérez
UpnaLab
Public University of Navarre
Pamplona, Spain
asier.marzo@unavarra.es
https://orcid.org/0000-0001-6433-1528

***Abstract*—LeviPrint assembles small objects in a contactless way using ultrasonic phased-arrays and optimization algorithms. We explore a set of methods that enables 6 Degrees-of-Freedom (DoF) control of elongated bodies. We then evaluate different ultrasonic arrangements to optimize the manipulation of these bodies. The combination of arrangements and optimization algorithms allow us to levitate, orientate and assemble complex objects. These techniques and arrangements can be leveraged for the microfabrication of electromechanical components and in-vivo additive manufacturing. We highlight the reduction of cross-contamination and the capability to manufacture inside closed containers from the outside.**

Keywords*—*acoustic hologram algorithm, 3D acoustic printer, acoustic levitation, acoustic tweezers, additive manufacturing.

I. Introduction

Acoustic levitation can hold, translate and rotate small objects of different materials without direct contact [5]. Multiple levitating primitives such as beads, threads, and fabrics have been used for assembling complex objects and articulated animated structures [2, 8, 9]. Rotation of sub-wavelength sized non-spherical particles has been achieved using an asymmetric acoustic field created with a phase-controlled transducer array[4]. Furthermore, phased-controlled arrays have been used to reach 3 DoF manipulation (2 translational DoF +

1 rotational DoF) of elongated bodies, like toothpicks [3]. However, 6 DoF manipulation of large elongated bodies (above-wavelength) has never been achieved. Here, we study different trapping techniques and phased-controlled arrays that enable full 6 DoF manipulation of large elongated bodies. Our method allows the translation and rotation of large items in any direction and any axes. In this poster, we propose the use of these techniques to attach beads and large items together as part of an additive manufacturing framework for building complex objects. This approach surpass current limitations of traditional additive manufacturing by reducing cross-contamination or manufacturing inside closed containers from the outside.

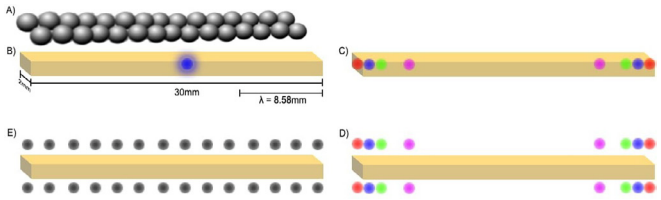

Figure 1. A) Stick approximated as a set of beads. B) Focal point at center of the stick. C) Focal points at sides. Different offsets used: Red=0mm; Blue=1mm; Green=2mm; Pink=5mm; D) Pairs of focal points at sides. Different offsets used: Red=0mm; Blue=1mm; Green=2mm; Pink=5mm; E) Twin wrapper method at 4 PPW (Pairs Per Wavelength).

II. Trapping methods

Arrays of transducers allow accurate generation of ultrasound fields that exert radiation forces on the levitation of particles. Algorithms for multi-point levitation calculate the phase delay for driving the array of transducers and creating a desire pressure field [6] capable of holding and manipulate midair elements. In this piece of work we propose and evaluate 12 different trapping methods for levitating and manipulating elongated bodies (See Fig. 1):

1) **Iterative Back Propagation (IBP) Methods:** These methods [6] generate multiple focal points.

- **At center:** One focal point is created at the center of the stick. The stick is levitated but not reoriented.
- **At sides:** Two focal points are created at the sides of the stick. Alternatives were tested offsetting the focal points 1mm, 2mm, 2.5mm and 5mm towards the center of the stick.
- **Pairs at sides:** Previously named *'at sides'* focal points are split into pairs. Alternatives were tested offsetting the focal points 1mm, 2mm, 2.5mm and 5mm towards the center of the stick.
- **Twin wrapper:** Previously named *'pairs at sides'* focal points are extruded along the stick with different distributions. 1, 2, 4 and 6 PPW (Pairs Per Wavelength).

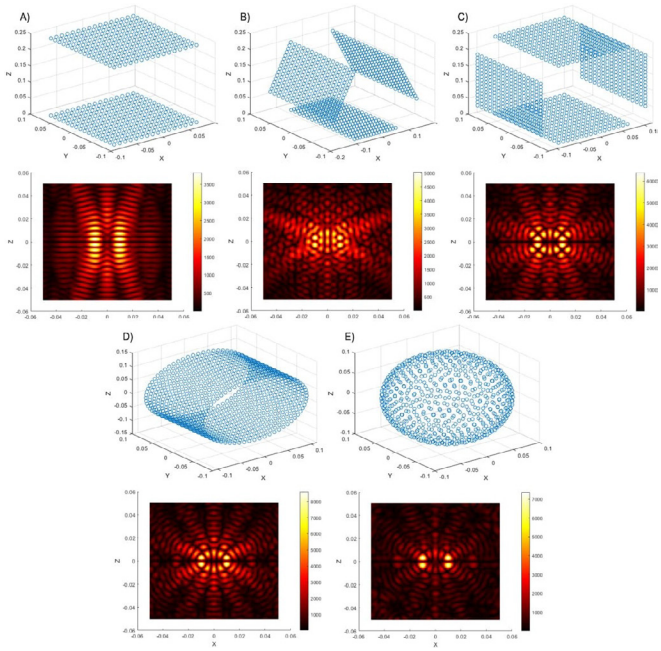

Figure 2. Transducers' arrangements simulated and a vertical slice of the pressure field that they create when applying IBP pairs at sides method. A) Two-opposed. B) Triangle. C) Cube. D) Cylinder. E) Sphere.

III. Transducers' arrangements

The quantity and distribution of the transducers plays a vital role in the manipulation capabilities of the final device. We have simulated and analyzed the behaviour of 5 different arrangements: 1) Two-opposed (512 transducers); 2) Triangle shaped (768 transducers); 3) Cube (1024 transducers); 4) Cylinder (1024 transducers); E) Sphere (642 transducers); See Fig. 2.

After benchmarking simulations of the setups, the two-opposed arrangement and the cube arrangement both were finally built to conduct experimental research with them. SonicSurface's Open Hardware Phased Arrays[7] were employed to build these devices. The cylinder and sphere arrangements were discarded, despite the good results shown in the simulations, because of the reduced working volume they offer towards additive manufacturing and their high complexity.

IV. Simulations and Conclusions

Forces, torques, Gor'kov potentials, positional stiffness and rotational stiffness were measured for a 30mm x 2mm stick placed in the center of the working volume when rotating it along each of its axes using the different IBP methods.

Positional Stiffness measures how converging are the forces in position, it is equivalent to the Laplacian of the potential. Rotational Stiffness measures how converging are the torques. The Gor'kov [1] potential for acoustic radiation pressure on a sphere is an approximation of the forces exerted on the sphere. The acoustic radiation forces push the particle towards the Gor'kov minimum potential.

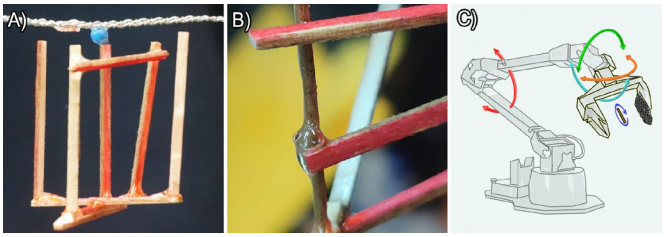

Figure 3. A) Photo of a large structure being built below the foundation. B) Photo of a solidified UV-cured glue droplet bonding two sticks together C) A 1-DoF rotation levitation device attached to a robot arm to perform precise movements and rotations.

As shown in Fig. 4.A), both methods, Twin Wrapper with 4 PPW and IBP at sides with 5mm offset appears to be the two preferred methods to be used for grabbing the stick caused by their low Gor'Kov potentials. Due to the high positional and rotation stiffnesses (Fig. 4 B, C and D), the cube arrangement appears to be a good alternative to the two-opposed arrangement for achieving the 90º rotations, critical for manufacturing vertical pieces and shorings.

V. Additive manufacturing

We illustrate the potential of Leviprint using varying numbers of primitives (sticks and beads), and making use of the different manipulations by our methods. The right combination of them will result in a robust structure that can be manufactured. Our methods will translate and position the primitives into their desired locations. Then, they will be fixed together by using an adhesive element. An acoustically transparent foundation should be placed in the center of the working volume before starting the building process as initial elements will be fixed to it (see Fig. 3.A). Applying spray glue was tested, however, it deliver excessive glue producing issues in the working volume such as stick areas and slow dry. Instead, we propose a new method using small droplets of UV-cured glue. A delivery mechanism (a syringe) delivers the glue which is levitated and placed accurately into the acoustic levitator. This method presents several benefits; it is cleaner, more precised, and easier than spraying glues (see Fig. 3.B). Additionally, these droplets can be used as a construction primitive on their own.

Finally, a robotic arm is proposed to hold a levitated device to speed up the manufacturing process. A custom levitator which generates a specific pressure field will be attached to the robot. (see Fig. 3). We note that the DoF in manipulations can be distributed between the robot and the levitator, e.g. Z-translation as well as rotation is performed by the levitator and the rest of the manipulation by the robot.

These new levitating manufacturing strategies will drastically reduce cross-contamination and they will offer the possibility to manufacture inside closed containers. Moreover, it enables manufacturing techniques not achievable with traditional 3D printing, such as threading through cavities or adding to the manufactured item towards any direction.

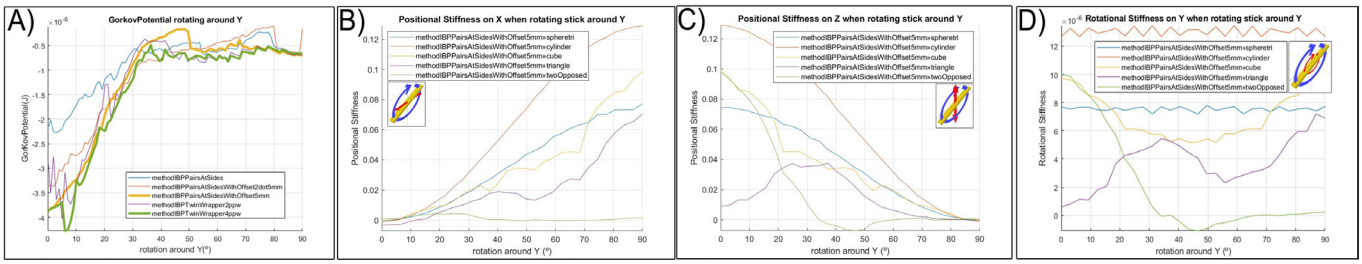

Figure 4. A) Gor'kov potential when rotating the stick along its Y axis. B) Positional Stiffness on the stick on axis X when rotating the stick around Y. C) Positional Stiffness on axis Z when rotating around Y. C) Rotational Stiffness over axis Y when rotating around Y.

Acknowledgment

This research was funded by the European Union's Horizon 2020 research and innovation programme under grant agreement No 101017746, TOUCHLESS.

References

[1] P Collas, M Barmatz, and C Shipley. Acoustic levitation in the presence of gravity. *The Journal of the Acoustical Society of America*, 86(2):777-787, 1989.

[2] Andreas Rene Fender, Diego Martinez Plasencia, and Sriram Subramanian. Articulev: An integrated self-assembly pipeline for articulated multi-bead levitation primitives. In *Proceedings of the 2021 CHI Conference on Human Factors in Computing Systems*, pages 1-12, 2021.

[3] Daniele Foresti, Majid Nabavi, Aldo Klingauf, and Dimos Poulikakos. Acoustophoretic contactless transport and handling of matter in air. *Proceedings of the National Academy of Sciences*, 110(31):12549-12554, 2013.

[4] Petteri Helander, Tuomas Puranen, Antti Meriläinen, Göran Maconi, Antti Penttilä, M Gritsevich, Ivan Kassamakov, Ari Salmi, Karri Muinonen, and Edward Haeggström. Omnidirectional microscopy by ultrasonic sample control. *Applied Physics Letters*, 116(19):194101, 2020.

[5] Asier Marzo and Bruce W Drinkwater. Holographic acoustic tweezers. *Proceedings of the National Academy of Sciences*, 116(1):84-89, 2019.

[6] Asier Marzo, Sue Ann Seah, Bruce W Drinkwater, Benjamin Sahoo, and Sriram Subramanian. Holographic acoustic elements for manipulation of levitated objects. *Nature communications*, 6(1):1-7, 2015.

[7] Rafael Morales, Iñigo Ezcurdia, Josu Irisarri, Marco AB Andrade, and Asier Marzo. Generating airborne ultrasonic amplitude patterns using an open hardware phased array. *Applied Sciences*, 11(7):2981, 2021.

[8] Rafael Morales, Asier Marzo, Sriram Subramanian, and Diego Martínez. Leviprops: Animating levitated optimized fabric structures using holographic acoustic tweezers. In *Proceedings of the 32nd Annual ACM Symposium on User Interface Software and Technology*, pages 651-661, 2019.

[9] Yoichi Ochiai, Takayuki Hoshi, and Jun Rekimoto. Pixie dust: Graphics generated by levitated and animated objects in computational acoustic-potential field. *ACM Trans. Graph.*, 33(4), jul 2014.

Optical biosensors: a quick overview

J.J. Imas
Electrical, Electronic and Communications Engineering Dept.
Institute of Smart Cities (ISC)
Public University of Navarra
Pamplona, Spain
josejavier.imas@unavarra.es

Carlos R. Zamarreño
Electrical, Electronic and Communications Engineering Dept.
Institute of Smart Cities (ISC)
Public University of Navarra
Pamplona, Spain

Ignacio R. Matías
Electrical, Electronic and Communications Engineering Dept.
Institute of Smart Cities (ISC)
Public University of Navarra
Pamplona, Spain

This work aims to provide a brief overview of the latest trends in the domain of optical biosensors. Biosensors are devices developed to obtain precise information from human body fluids, such as plasma, blood or urine, among others. Their main elements are the bioreceptor, that binds the biomarker (the target molecule); and the transducer, which is intimately linked to the bioreceptor and provides a measurable response. The main bioreceptors comprise antibodies, enzymes, nucleic acids and molecularly imprinted polymers. Previously mentioned bioreceptors can be immobilized on the sensor surface using different techniques including physical adsorption, covalent binding, physical entrapment in a hydrogel or chemical cross-linking[1].

Regarding optical transducers, interrogation techniques primarily consist of light-intensity, phase, and frequency or polarization modulations caused by the bioreceptor in the presence of the biomarker. Optical biosensors possess increasing relevance as a result of their advantages, including their capability of a direct, real-time and sometimes label-free detection, as well as their high specificity, sensitivity, compact size and good cost-performance ratio[2]. The most widely used optical biosensors are those based on surface plasmons, fluorescence, interferometry, whispering gallery modes and photonic crystals.

Surface plasmons are electromagnetic excitations that propagate along the interface between a dielectric medium and a metal. In the presence of the biomarker, the refractive index in the region adjacent to the biosensor surface changes, therefore varying the resonant wavelength, the intensity and/or the phase of the light coupled to the surface plasmons. By monitoring one of these variables, such as the resonant wavelength in surface plasmon resonance (SPR) based biosensors, the concentration of the analyte can be obtained[3]. SPR stands out for having high sensitivity and enabling direct and real-time monitoring of the analyte binding[4]. Similar to SPRs, lossy mode resonances (LMRs) are generated when a metal oxide or polymer is used instead of a metal. LMRs have a higher sensitivity than SPRs, making them ideal for the development of biosensors.

SPR imaging (SPRi) differs from conventional SPR in incorporating a CCD (charge-coupled device) camera that enables sensorgrams and SPR images to be recorded at the same time; while SPR microscopy (SPRM) adds a high numerical aperture lens for light coupling, allowing single molecule detection. Finally, long range SPR (LRSPR), with thin films 20-25 nm thick, possess an increased sensitivity thanks to the low propagation loss and deeper field penetration[5]. In the case of localized surface plasmon resonances (LSPR), the plasmons oscillate locally to a nanostructure (such as nanoparticles) instead of along the dielectric-metal interface. The high electromagnetic fields around the nanostructure induce an increase in sentitivity[6].

Fluorescence sensors consist basically of using a light source at an excitation wavelength to excite a fluorophore or label and measuring the fluorescent response at the peak wavelength[7]. In the case of biosensors, the sensing mechanism links the analyte concentration with the fluorophore concentration. Fluorescence biosensors are characterized by a high sensitivity and specificity while their drawbacks are those associated with the use of fluorophores, including photobleaching or self-quenching. In general, fluorescence biosensors operation is based on sandwich immunoassays where the second antibody is labeled with a fluorophore.

Waveguide interferometric sensors are based on the light travelling through two different paths. Here, one path is used as reference, where the light propagates without suffering any alteration. Then, the sample is placed along the other path inducing a phase shift. The interference of the modes that travel through both paths produces a signal that is related to the analyte concentration[8]. The most commonly used interferometers in biosensing applications are the Mach-Zehnder (MZI) and the Young (YI) interferometers[5].

In the case of the MZI, the incident monochromatic light is split into two arms by a Y-junction and both beams are then recombined with another one. Modifications of the MZI basic structure include the use of slot waveguides in the sensing arm to increase the sensitivity and the integration in compact devices of several MZIs for multisensing[5]. The YI differs from the MZI in lacking the second Y-junction. In this interferometer, the light from the reference and the sensing arms diffracts and interferes on an image sensor such as a CCD camera.

Whispering-gallery modes (WGM) are electromagnetic waves that circulate and are strongly confined in a dielectric structure with circular symmetry, producing resonances through internal interference. This structure is resonantly stimulated by evanescent coupling to a waveguide. The obtained resonances have a narrow full-width at half maximum (FWHM), thus obtaining a high resolution.[9] The most widely employed WGM resonators in biosensing are microsphere resonators, which are easy to fabricate but difficult to integrate; and planar microring resonators, which are robust, compact and suitable for multiplexing and integration but have lower sensitivities[5].

Photonic crystal (PC) structures consist of spatially arranged periodic dielectric materials in which light is highly reflected at specific wavelengths. PC structures can be manufactured in one (1-D), two (2-D) or three (3-D) dimensions,

incorporating microcavities, waveguides, slabs, multilayered thin films or porous geometries, and employing materials such as silicon, glass, polymers, colloids or silk. They are fabricated through various techniques such as self-assembly or lithography and their advantages include compact size, flexible configuration, high sensitivity and the possibility of monolithic integration.[10]

In conclusion, different types of biosensors have been described focusing on the optical sensing techniques. Nevertheless, most of these configurations have been developed only for their use in the laboratory and further developments are required in order to obtain reliable, high-sensitive and low cost point of care devices for disease monitoring and diagnosis.

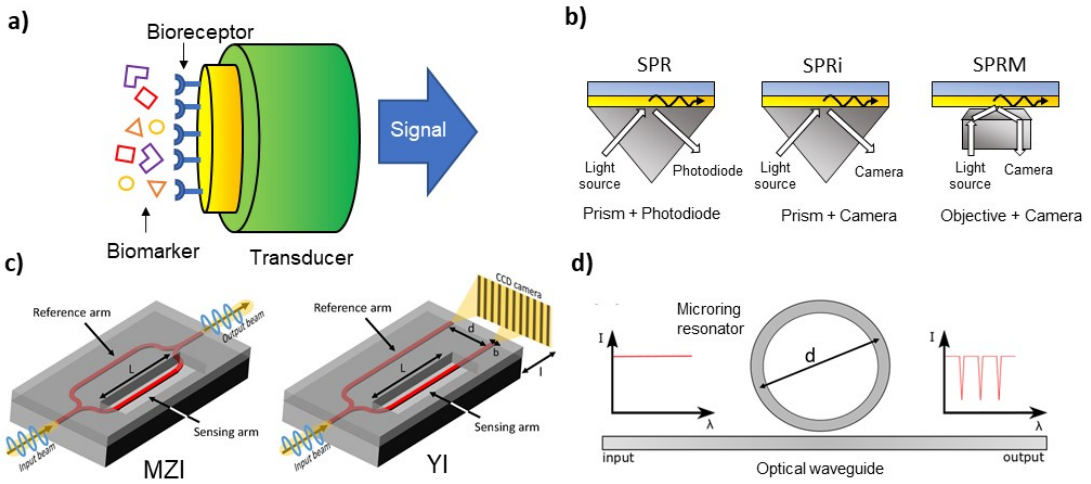

Figure 1. a) Schematic of a biosensor. b) Three types of SPR configuration. c) Schematic of MZI and YI configurations, adapted.[11] Reproduced under the terms of the Creative Commons Attribution license d) Schematic of a microring resonator, adapted.[12] Reproduced under the terms and conditions of the Creative Commons Attribution license.

Acknowledgements

We want to thank the funding from Ministerio de Ciencia, Innovación y Universidades (FPU18/03087) and Agencia Estatal de Investigación (PID2019-106231RB-I00 TEC).

References

[1] Chen, C. & Wang, J. Optical biosensors: An exhaustive and comprehensive review. *Analyst* vol. 145 1605-1628 (2020).

[2] Damborský, P., Švitel, J. & Katrlík, J. Optical biosensors. *Essays Biochem.* **60**, 91-100 (2016).

[3] Špačková, B., Wrobel, P., Bocková, M. & Homola, J. Optical Biosensors Based on Plasmonic Nanostructures: A Review. *Proceedings of the IEEE* vol. 104 2380-2408 (2016).

[4] Singh, P. SPR Biosensors: Historical Perspectives and Current Challenges. *Sensors and Actuators, B: Chemical* vol. 229 110-130 (2016).

[5] Chen, Y., Liu, J., Yang, Z., Wilkinson, J. S. & Zhou, X. Optical biosensors based on refractometric sensing schemes: A review. *Biosens. Bioelectron.* **144**, 111693 (2019).

[6] Hammond, J., Bhalla, N., Rafiee, S. & Estrela, P. Localized Surface Plasmon Resonance as a Biosensing Platform for Developing Countries. *Biosensors* **4**, 172-188 (2014).

[7] Strianese, M. *et al.* Fluorescence-based biosensors. *Methods Mol. Biol.* **875**, 193-216 (2012).

[8] Kozma, P., Kehl, F., Ehrentreich-Förster, E., Stamm, C. & Bier, F. F. Integrated planar optical waveguide interferometer biosensors: A comparative review. *Biosensors and Bioelectronics* vol. 58 287-307 (2014).

[9] Righini, G. C. *et al.* Whispering gallery mode microresonators: Fundamentals and applications. *La Riv. del Nuovo Cim. 2011 347* **34**, 435-488 (2011).

[10] Inan, H. *et al.* Photonic crystals: Emerging biosensors and their promise for point-of-care applications. *Chem. Soc. Rev.* **46**, 366-388 (2017).

[11] Luan, E., Shoman, H., Ratner, D. M., Cheung, K. C. & Chrostowski, L. Silicon photonic biosensors using label-free detection. *Sensors (Switzerland)* vol. 18 (2018).

[12] Steglich, P., Hülsemann, M., Dietzel, B. & Mai, A. Optical Biosensors Based on Silicon-On-Insulator Ring Resonators: A Review. *Mol. 2019, Vol. 24, Page 519* **24**, 519 (2019).

SMARTERIAL – Smart matter optomagnetic

Josu Irisarri Erviti
Dept. Statistics, Computer Science and Mathematics
UPNA (UPNALAB HCI research group)
Pamplona, Spain
josu.irisarri@unavarra.es
https://orcid.org/0000-0001-8783-7732

Xabier Sandua Fernández
Dept. Engineering
UPNA (Institute for Advanced Materials and Mathematics)
Pamplona, Spain
xabier.sandua@unavarra.es
https://orcid.org/0000-0002-5156-4784

Itziar Galarreta Rodríguez
Dept. Science
UPNA (Institute for Advanced Materials)
Pamplona, Spain
itziar.galarreta@unavarra.es
https://orcid.org/0000-0001-9172-4319

Asier Marzo Pérez
Dept. Statistics, Computer Science and Mathematics
UPNA (UPNALAB HCI research group)
Pamplona, Spain
asier.marzo@unavarra.es
https://orcid.org/0000-0001-6433-1528

***Abstract*—Smart materials, also known as programmable materials, are a combination of different components that have the capability to change shape, move around and adapt to numerous situations by applying an external controllable field. Previous works have used optically guided matter or magnetically actuated materials, but similarly to soft robots, they are limited in spatial resolution or strength. Here we propose combining a low temperature thermoplastic polymer Polycaprolactone (PCL) with ferromagnetic powder particles (Fe). Focused light can heat this compound at specific locations and make it malleable. These heated spots can be actuated by external magnetic fields. Once the material cools down, this process can be repeated, or reversed. The compound can be actuated contact-less in the form of 3D slabs, 2D sheets, and 1D filaments. We show applications for reversible tactile displays and manipulation of objects. The laboratory team has characterised the density, weight, magnetic attraction, magnetic force, phase change, thermal and electrical conductivity and heat diffusion (spread point test) for smart ferromagnetic compounds of different mixture proportions. The main advantages of this smart matter optomagnetic are the high spatial resolution of light and the strong force of magnetic attraction whilst mechanical properties of polymers are practically conserved. Due to the low temperature required and the possibility to use infrared or electromagnetic induction to heat the compound, the smart material can be used in air, water, or inside biological tissue. Eventually, smart materials will enrich collaborative movements, such as grab and hold, and more complex ones, as reshaping and reassembling.**

Keywords*—Material Science, Programmable materials, Silly Putty, Haptics, Soft Robots, Magnetic and Thermal Control

I. Introduction

The excellent malleability that thermoplastic exhibits at certain temperatures combined with the ferromagnetic property that includes Fe particles throughout the matrix, make this component an interactive material by applying a magnetic field.

Public University of Navarre (UPNA) and European Union's Horizon 2020 research and innovation programme (TOUCHLESS)

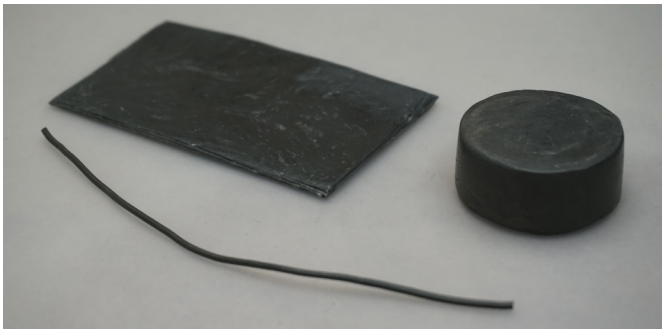

Figure 1. Three different dimensional samples of smarterial. Crafted 3D slab, 2D sheet and 1D filament.

By the application of specific heat sources on the material, these areas of the composite become malleable. Taking into account this property offered by the mixture, a magnetic field is applied to these areas, through a certain gradient of permanent magnets, which will be in charge of attracting the Fe particles that are located within the matrix. The malleable state of the PCL allows the Fe particles to move attracted by the magnetic field, dragging with them the polymeric material and thus modifying the shape of the compound.

This phenomenon allows a large number of applications ranging from the instantaneous formation of Braille code to the printing of different shapes in the same matrix, depending on the thermally altered area and the shape of the subsequent magnetic field applied to the material. Not only is it interesting to build a matrix with this compound, but there are also elements such as filaments and surfaces, with which you can interact in the same way as described for the matrix.

Figure 2. 3D sculpting, 2D patterning (e.g. Braille code) and 1D lettering.

II. Related work

Previous research have shown the high performance that this type of materials are capable of. Millimetre-scale flexible robots[[5]] or small-scale soft continuum robots[2] seems to be the state of the art. These technology came out as a result of the intention to discover a new innovative method to combine human body and robots. Imaging how it is introduced and controlled inside our organism is truly a step forward for medicine. Cargo delivery microswimmer[3], a self-assemble origami robot that can recycle itself[6], multimodal locomotion soft-bodies[1] or insect inspired robots[4] are examples reachable for this material.

III. Methods

The present characterization includes different proportion samples depending on their percentage of iron (Fe) inside the mixture (from 1 to 5). Moreover, the compounds were crafted either by manual transforming (M) or by chemical synthesis (C). Next table expose the compounds of the right picture, following the order from left to right of the both rows:

TABLE I. Iron (Fe) proportions inside the compounds

Iron (Fe)	10%	20%	30%	40%	50%
M (%)	M1	M2	M3	M4	M5
C (g)	C1	C2	C3	C4	C5

A. *Thermal conductivity*

All samples have been placed on a hot-bed at 50ºC. The temperature of each compound have been recorded by a thermal camera RS T-10. It demonstrates that the more iron, the more thermal conductivity the material has. Bear in mind that this also affects the cool-down.

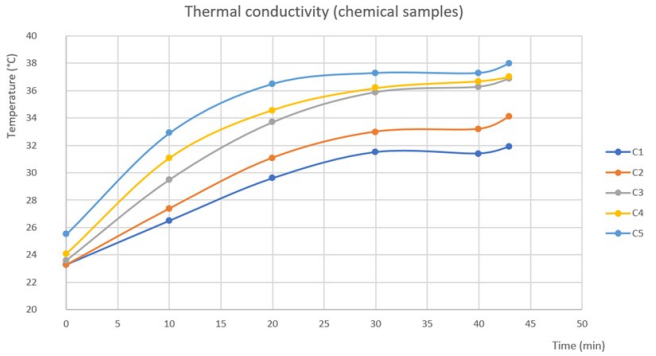

Figure 3. Thermal conductivity results of chemical samples

B. *Magnetic force*

For this experiment, each sample has been subjected to a vertical force (F), perpendicular to its surface, while on a magnet hanging from a weight scale. Chemical samples C4 and C5 reached more than 5kg.

C. *Electrical conductivity*

Electrical resistance could be measured by a digital multimeter VC60B+ in two of the samples, C4 and C5. Used as a conductor, C5 can turn on a LED due to its 30kΩ, resistance.

C4 has around 400MΩ, while all other samples have more than 2000MΩ, which is the limit of the ohmmeter.

IV. Discussion and future work

Laboratory team strongly believes that this kind of intelligent materials will have high impact in the society for new innovative incoming technologies. It has the potential to break into novel fields such as assisted physiotherapy, medicine, volumetric displays or even as a new artistic movement.

Acknowledgment

This research was funded by the European Union's Horizon 2020 research and innovation programme under grant agreement No 101017746, TOUCHLESS.

References

[1] Wenqi Hu, Guo Zhan Lum, Massimo Mastrangeli, and Metin Sitti. Small-scale soft-bodied robot with multimodal locomotion. *Nature*, 554(7690):81-85, 2018.

[2] Yoonho Kim, German A Parada, Shengduo Liu, and Xuanhe Zhao. Ferromagnetic soft continuum robots. *Science Robotics*, 4(33), 2019.

[3] Mariana Medina-Sánchez, Lukas Schwarz, Anne K Meyer, Franziska Hebenstreit, and Oliver G Schmidt. Cellular cargo delivery: Toward assisted fertilization by sperm carrying micromotors. *Nano letters*, 16(1):555-561, 2016.

[4] Owies M Wani, Hao Zeng, and Arri Priimagi. A light driven artificial flytrap. *Nature communications*, 8(1):1-7, 2017.

[5] Tianqi Xu, Jiachen Zhang, Mohammad Salehizadeh, Onaizah Onaizah, and Eric Diller. Millimeter-scale flexible robots with programmable three-dimensional magnetization and motions. *Science Robotics*, 4(29), 2019.

[6] Haitao Yang, Bok Seng Yeow, Zhipeng Li, Kerui Li, Ting-Hsiang Chang, Lin Jing, Yang Li, John S Ho, Hongliang Ren, and Po-Yen Chen. Multifunctional metallic backbones for origami robotics with strain sensing and wireless communication capabilities. *Science Robotics*, 4(33), 2019.

Coupling in multilayer devices

Eduardo Jarauta
Electrical Engineering Departament
Public University of Navarre
Pamplona, Spain
jarauta.31784@e.unavarra.es

Francisco Falcone
Institute of Smart Cities
Public University of Navarre
Pamplona, Spain
francisco.falcone@unavarra.es

***Abstract*—Novel design for devices in multilayer stacked is proposed. Split Ring resonators and Complementary Split Ring resonators are used, in microstrip or dual stripline-microstrip configuration to build different devices. A double frequency resonator and a multilayer triplexer are presented among the paper.**

Keywords—coupling, SRR, CSRR, multilayer

I. Introduction

The properties of Split Ring Resonators (SRR), studied at the end of last century by [Pendry], as well as Complementary Split Ring Resonators proposed by [Falcone] established a starting point for the design of novel microwave devices. The operation in sub-lambda operation for these particles made them suitable in the miniaturization of microwave devices such as filters [Bonache], couplers [Jarauta] or antennas [Paul].

In this paper Square Complementary Split ring Resonators (SCSRR) will be used instead. The main dimensions can be seen in Fig.1 They are square side length *l*, width of the rings *c*, and separation between rings *d*.

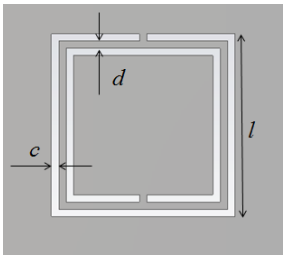

Figure 1. SCSRR main dimensions

II. Double frequency resonator

For the first device, the serial resonator proposed in [Jarauta] is taken as started point. There, a Square SRR (SSRR) in serial resonator is used. The SSRR in the serial configuration is excited because of the electric field perpendicular to the microstrip line, due to the bi-anisotropy of SSR [Marques Iddrisi]. Just below SSRR, a Square CSRR (SCSRR) is etched in the metallization layer. This resonator is excited due to the e-field established from input line to the ground in microstrip line. The layout and the top layer of fabricated prototype are shown in Fig.2.

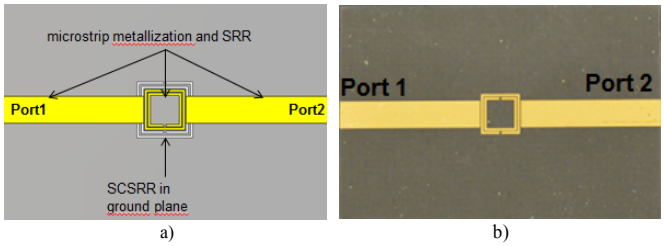

Figure 2. a) Top view overlapped layers. b) Top layer manufactured prototype

This device was designed in the commercial substrate Rogers RO5880 with thickness h=0.79mm. The SSRR on top layer has a side length l_1 = 3,4mm, width of the rings c = 0,2mm, separation between rings d = 0,1mm and distance between microstrip input and SSRR s_1 = 0,1mm. The SCSRR has a side length l_2 = 5mm, width of the rings c_2 = 0,2mm, separation between rings d_2 = 0,1mm. In the case of SCSRR is also important to consider the length of input metallization line over the SCSRR. In this case defined from the center of the ring to the beginning of the metallization layer as p_1 and p_2 as plotted in Fig 3.

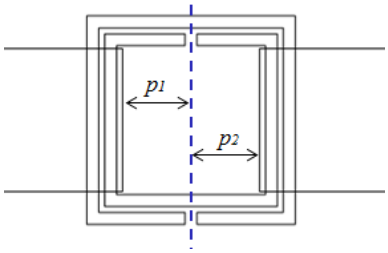

Figure 3. Detailed parameters p1 and p2 over the SCSRR

For the device in Fig. 2, the parameters are p_1 = 1,9mm and p_2 = 1,9mm. With all above dimensions, the simulation results can be seen in Fig.4.

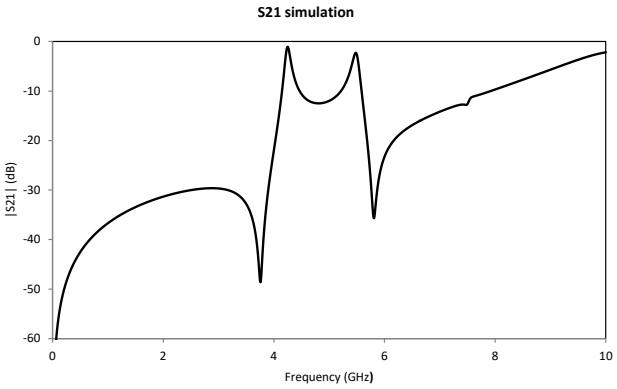

Figure 4. Simulated S_{21}.

Two resonances are obtained, the first one at f1= 4,24GHz, corresponding to the CSRR resonance with a value S21=1,2dB. The second one at f2=5,51GHz is the resonant frequency of the SSRR. In this case the insertion loss S21=1,1dB.

III. Multilayer stripline diplexer

The second device proposed is a multilayer diplexer. The input line is a stripline. On both metallization layers which builds the stripline groundplane, a couple of SCSRRs are etched. As it is well known, in a stripline a TEM mode Finally, over and below of each metallization layer, a new substrate

with a new strip just above the side of the rings is located. They build two microstrip lines that act as output layers. The different layers are schematically displayed in perspective view in Fig. 5a and in front view in picture Fig. 5b.

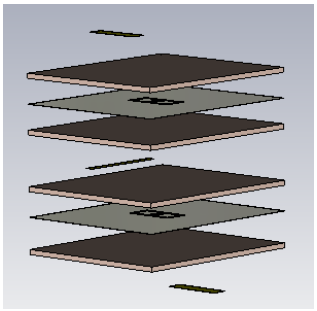

a)

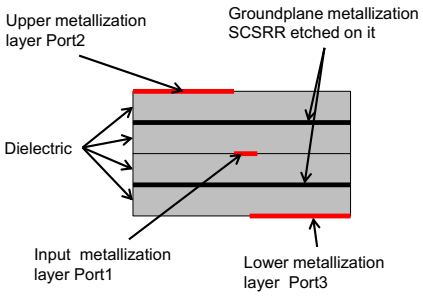

b)

Figure 5. Multilayer stripline diplexer. a)perspective view. b) front view

The SCSRRs are identical and they are positioned side by side as it can be seen in Fig. 6. The main dimensions are l=4mm, c=0,2mm, d=0,2mm. Separation between rings is s=0,2mm. The values of the distance from the center of the SCSRR to the beginning of output line to port 3 is p_1=1,5mm. And to port 4, p_2=1,4mm. The design details can be seen in top view in Fig. 6.

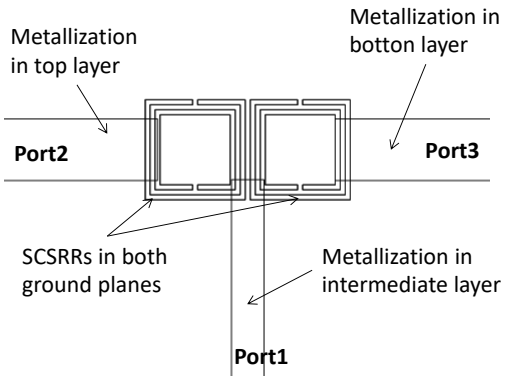

Figure 6. Multilayer stripline diplexer top view

The results of simulation for device presented can be seen in Fig. 7.

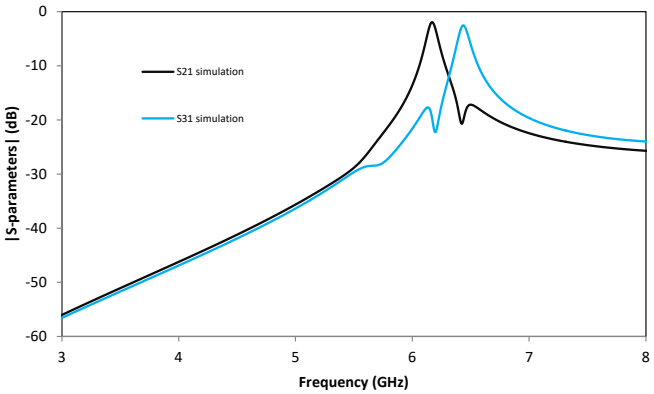

Figure 7. S-parameters response for multilayer diplexer

The S-parameters response for this device presents two resonant frequencies. The first one, to output port 2, f_0=6,176GHz with insertion loss S_{21}=-2,02dB and the second one to output in port 3 is achieve at f_1=6,44GHz with insertion loss S_{31}=-2,56dB. Two remarkable results are obtained for this device. Good insertion losses on each port, but also, that resonant frequencies are really close each other.

IV. Discussion of the results

It is possible the coupling of energy between layers vertically. The effective area for the double resonator is 0,0019 λg^2. For the case of the diplexer apart from the insertion losses, a key figure is the separation between resonant frequencies with a ratio of 1,043.

References

[1] J. B. Pendry, A. J. Holden, D. J. Robbins, y W. J. Stewart, «Magnetism from conductors and enhanced nonlinear phenomena», *IEEE Transactions on Microwave Theory and Techniques*, vol. 47, n.º 11, pp. 2075-2084, nov. 1999, doi: 10.1109/22.798002.

[2] F. Falcone, T. Lopetegi, J. D. Baena, R. Marques, F. Martin, y M. Sorolla, «Effective negative-epsiv; stopband microstrip lines based on complementary split ring resonators», *IEEE Microwave and Wireless Components Letters*, vol. 14, n.º 6, pp. 280-282, jun. 2004, doi: 10.1109/LMWC.2004.828029.

[3] J. Bonache, I. Gil, J. Garcia-Garcia, y F. Martin, «Novel microstrip bandpass filters based on complementary split-ring resonators», *IEEE Transactions on Microwave Theory and Techniques*, vol. 54, n.º 1, pp. 265-271, ene. 2006, doi: 10.1109/TMTT.2005.861664.

[4] E. Jarauta et al., «Novel microstrip backward coupler with metamaterial cells for fully planar fabrication techniques», Microw. Opt. Technol. Lett., vol. 48, n.º 6, pp. 1205-1209, jun. 2006, doi: 10.1002/mop.21579.

[5] P. M. Paul, K. Kandasamy, y M. S. Sharawi, «A Triband Circularly Polarized Strip and SRR-Loaded Slot Antenna», IEEE Transactions on Antennas and Propagation, vol. 66, n.º 10, pp. 5569-5573, oct. 2018, doi: 10.1109/TAP.2018.2854911.

[6] E. Jarauta, F. Falcone, y M. Beruete, «High-Q series coupled microstrip split-ring resonator device», Waves in Random and Complex Media, vol. 24, n.º 2, pp. 218-226, abr. 2014, doi: 10.1080/17455030.2014.904534.

[7] R. Marqués, F. Medina, y R. Rafii-El-Idrissi, «Role of bianisotropy in negative permeability and left-handed metamaterials», *Phys. Rev. B*, vol. 65, n.º 14, p. 144440, abr. 2002, doi: 10.1103/PhysRevB.65.144440.

Implementation of artificial intelligence algorithms in climatic zoning according with energy demand in dwellings. A european case

Javier Llorente
UPNA Public University of Navarre
Pamplona, Spain
llorente.39047@e.unavarra.es

Laura Frías
UPNA Public University of Navarre
Pamplona, Spain

Martín Gastón
UPNA Public University of Navarre
Pamplona, Spain

Hassam ur Rehman
VTT Technical Research Centre of Finland Ltd.
Finland

I. Introduction

Science has shown, based on data and knowledge, that there is clear evidence that global warming is not a transient effect, and that it is caused mainly by human activity [1]. The consequences of climate change can be noted and quantified nowadays [2], but the worst thing is that these impacts are expected to intensify in the coming decades. Obviously, global problems require global solutions, and even if there are certain difficulties to define a clear path, there is no doubt that the worldwide efforts should lead to keep the global temperature increase to well below 1.5ºC [3].

Greenhouse gases (GHG) have a major influence on global warming, and they are mostly emitted as a consequence of anthropogenic processes which are linked with the high energy consuming society, low energy efficient systems and the use of fossil fuels as primary energy. In this sense, in the European Union (EU), buildings are responsible for 40% of the energy consumption and 36% of GHG emissions [5]. By the year 2018, households accounted for 26.1% of final energy consumption in the EU, being the main use of energy to maintain adequate comfort conditions [4].

Then, it is clear that in order to achieve the ambitious goal of carbon neutrality by 2050 [6], improving the energy efficiency in buildings has to play a key role. Given the fact that most of the energy use is employed in satisfying the heating and cooling demands, there is a clear dependence between weather or climate conditions and energy consumption in the buildings. However, there is no climatic zoning of Europe which would be of high importance to define clear objectives in terms of energy consumption in buildings; to allow the replication of successful experiences with low energy consumption in similar weather conditions; and to define realistic energy plans.

Buildings are part of districts, and being Positive Energy Districts [7] the intermediate step between positive energy building and positive energy city, the results from the research could be of high interest.

II. Methods

So far, the climatic zoning for energy demand in buildings in different EU Members States do not follow a common pattern or methodology. In fact, being an issue which apparently does not require many input data, it could be reasonable to think that the climatic zoning in Europe has already been developed.

There are 3 main methodologies to define the climatic zoning. One of these methodologies employs the Köppen-Geiger classification [8] which has been employed for many different applications and is the most employed worldwide so far. This classification takes into consideration temperature and rain precipitation, and clearly classifies the weather conditions based on defined thresholds. There are 5 main climate zones and up to 30 subzones, and it is really useful for vegetation purposes. The second type of methodologies takes into consideration the Degree-Days (DD) concept [9], both for Heating (HDD) and Cooling (CDD) purposes. However, the threshold values for the HDD and CDD calculations vary and so does the threshold values for the classifications. ASHRAE standard 169-2013 [10] defines a climatic classification based on HDD and CDD, but despite the fact of being a methodology easy to calculate and understand, it does not consider other input values such as solar radiation. Finally, the third kind of methodologies are based on the definition of Severity Climate Indexes for Winter (WCS) and Summer (SCS) obtained from the use of energy simulation calculations. These methodologies require the use of computational resources and are difficult to understand, since are based on mathematical modelling. Spain's climatic zoning was defined based on Severity Climate Indexes.

Then, the objective of the research is to follow the Montecarlo method and run a huge number of parametric energy simulations varying the most influence variables (air infiltration, wall insulation, orientation...), and making use of Artificial Intelligence define the number and the boundaries of the climatic zoning in Europe.

III. Main Results

When comparing the different methodologies, there are several inconsistencies among the results from the methods when using the typical meteorological years from several locations in Europe. The main issue is to classify correctly the "intermediate" climates, since hot and cold climates are simple to classify. However the definition of a clear boundary between the zones varies from one method to another, and so does the number of zones.

After a total of 88,704 energy simulation run with TRNSYS software [11], it is clear that there is a dependence of energy demand in buildings on solar radiation, so the climatic

classification to be defined should consider this variable on the calculations.

HDD and CDD are good predictors, but the performance is increased when another variable such as solar radiation is employed.

IV. Discussions

A common approach should be employed, in order to be able to compare results from similar weather conditions. Nowadays, two countries with apparently similar climates (Spain and Italy), employ different methodologies in climatic zoning, although it should be easier to define the climatic zones in those countries. When this issue is extrapolated to the EU, it seems more obvious to have a common strategy towards a common objective.

Some of the methodologies employed so far lack of accuracy, and this leads to a variety of results among them.

This way, a minimum of 5 climatic zones have to be defined in Europe.

V. Future Work

The first results from the parametric study showed good performance. The future work is to define a number of different buildings based on the typology (block of apartment, detached houses, etc) and the comfort conditions considering the comfort levels in different European countries.

An update of weather climates based on recent weather data has to be done, because most of Typical Meteorological Years need periods of time longer that 20-25 years, and in the last years the weather has varied. As a consequence of global warming, HDD (and therefore heating demand) is decreasing, and the opposite occurs to CDD (and Cooling Demand).

The authors will investigate about the most appropriate AI techniques to carry out the most suitable climatic zoning in Europe. These developments will help to define the planning of the building sector pathways considering energy, CO_2 emissions and economic savings under a common strategy.

References

[1] https://www.ipcc.ch/2021/08/09/ar6-wg1-20210809-pr/

[2] https://ec.europa.eu/clima/change/consequences_en

[3] https://unfccc.int/conference/glasgow-climate-change-conference-october-november-2021

[4] https://ec.europa.eu/eurostat/web/products-eurostat-news/-/DDN-20200626-1

[5] https://ec.europa.eu/info/news/focus-energy-efficiency-buildings-2020-feb-17_en

[6] https://ec.europa.eu/info/strategy/priorities-2019-2024/european-green-deal_en

[7] https://annex83.iea-ebc.org/subtasks#Subtask%20B

[8] http://koeppen-geiger.vu-wien.ac.at/pdf/Paper_2017.pdf

[9] https://ec.europa.eu/eurostat/statistics-explained/index.php?title=Heating_and_cooling_degree_days_-_statistics

[10] https://www.techstreet.com/ashrae/standards/ashrae-169-2013?gateway_code=ashrae&product_id=1869436

[11] http://www.trnsys.com/

Contributions of Artificial Intelligence to low resolution Renal Multiparametric Magnetic Resonance Analysis

Anne Oyarzun Domeño
Electrical, Electronics and Communications Engineering
Public University of Navarre
Pamplona, Spain

Arantxa Villanueva Larre
IdiSNA, Instituto de Investigación Sanitaria de Navarra
ISC, Institute of Smart Cities
Pamplona, Spain

***Abstract*—Arterial spin labeling (ASL), is a Multiparametric Magnetic Resonance Imaging (MRI) technique used to quantify and evaluate Renal Blood Flow (RBF) and detect perfusion failure by labelling blood water as it flows throughout the kidney. This study aims at providing an automatic quantifying and evaluation tool for Chronic Kidney Disease (CKD) patients's follow-up.**

I. Introduction

Chronic Kidney Disease (CKD) is a conditon characterized by a gradual loss of kidney function over time [1]. It is estimated that the 10% of the population suffer from CKD and is expected to continue to grow, due to aging and increased incidence of diabetes and obesity. In patients with advanced CKD, renal transplant improves quality of life and increases survival rate. In recent years, the incidence of acute rejection has been considerably reduced and early loss of implant has been minimized. However, the causes of the progressive deterioration of the implant are various and its mechanisms are unknown. For that reason, postoperative renal implant evaluation is a complex diagnostic problem.

In the presented research project, dataset from 18 renal transplanted patients was used, approved by the Ethics Research Committee of the University of Navarra. ASL-MRI scans were performed on a 3T Skyra using an 18-channel body-array coil. Perfusion images were acquired using a *pseudo continuous arterial spin labeling (PCASL)* sequence [2].

II. Motion-Correction Techniques

Motion correction methods are a prerequisite in multiple-image registration tasks. We implemented a non-rigid group-wise registration with PCA2 metric [3]. The method aligns volumes on a slice-wise basis. We compared the registration method without focusing on a *Region of Interest (ROI)* and within a ROI. The ROI in each slice of the volume was manually marked and subsequently dilated to encompass whole renal area. The registration was implemented in Elastix [4].

After image registration, *Perfusion Weighted Images (PWI)* maps were extracted by subtracting registered control and label images.

Temporal Signal to Noise Ratio (tSNR) was computed as the ratio of the mean to the temporal standard deviation, as a measure of signal stability. Outliers were discarded when the ASL signal was more than 2 standard deviations (SD) away from the global mean [2]. Manually defined and sub-sequently eroded ROI on the cortex was used to measure the tSNR along ASL pairs. Motion correction techniques show statistically significant improvement ($p<0.025$) on the tSNR. No statistical difference was found between two registration approaches in terms of temporal signal variation of the images ($p>0.025$). However, our dataset presents high inter-subject variability, to which groupwise registration method is highly dependent on. For that reason, for those tSNR samples higher than mean tSNR, RR method shows statistically significant difference ($p<0.025$) on tSNR mean, compared to NRR method, indicative of a more successful image alignment.

III. Kidney Segmentation

Kidney parenchyma's segmentation serves as quantitative analysis [5] tool for renal damage prevention, which requires time-consuming pixel-wise annotation. Nonetheless, *Machine Learning (ML)* based medical image segmentation has shown its value in segmentation of several organs. *Supervised Descent Method (SDM)* is a cascaded regression approach that learns generic descent directions in a supervised way [6]. Besides, the *U-NET* is a widely used non-supervised *Convolutional Neural Network* for medical image segmentation. It consists of a contracting path to capture context and a symmetric expanding path that enables precise object localization [7]. We proposed the *Cascaded Weighted UNET-SDM (CUS)* model, consisted on the automation of SDM for kidney segmentation, based on preliminary trained UNET's result initialization.

First, the UNET was trained on augmented data and introduced sample weights in the Dice loss function. It was minimized via *Adam* optimizer and learning rate of 1x10-

4, with a batch size of 16 and 100 epochs. Training and testing of the model was implemented on Python 3.8 using Tensorflow as backend on GPU NVIDIA GeForce RTX 3090. Secondly, we used *Histogram of Gradient (HOG)* extraction to encode local shape information from point locations within the image. We used 40 landmarks and 100 initializations. Initial shapes for training were translated ground truth masks with additional independent noise applied to each landmark and testing was performed on kidneys' mean shapes. The algorithm was implemented in Matlab on Intel(R) Core(TM) i5-7500 CPU.

The prediction accuracy of CUS was evaluated in terms of *Dice Score (DS)* similarity index. Proposed architecture achieved statistically higher score mean compared to original UNET ($p<0.005$). Besides, it showed an outstanding segmentation accuracy ($DS = 0.850 \pm 0.028$) and statistically higher performance, comparing with the original UNET. These accurate image segmentation models enable functional and struc-

tural information extraction, including kidney detection and shape estimation.

Discussion

Our results demonstrated the applicability of both groupwise registration and parenchyma's segmentation process on postoperative renal implant evaluation. We achieved to counteract the misregistration of control and label images to subsequently extract whole kidney mask for each image. Furthermore, the kidney detection process serves as a reference for further RBF calculation methods.

IV. Challenges and Future Work

The implementation done in these initial steps has provide a good starting point for further research.

Coarse-to-Fine Segmentation

Innovative Coarse-to-Fine approach could be performed to improve ML based segmentation results. Mask R-CNN is a pixel-based Instance Segmentation model that adds an extra parallel branch on Faster-RCNN to segment instances within predicted boxes [8]. Renal ASL-MRI are low resolution images and present other highlighted organs as the bladder, which worsens the final segmentation result. The implementation of these kind of models could improve kidney's edge detection, from firstly detected kidney's bounding box. The training process should be adapted to volumetric grayscale data.

Segmentation of Renal Compartments

The segmentation of renal cortex and medulla has its value on functional kidney evaluation. Despite the development of tools for the segmentation of entire kidney, there is a lack of renal compartments segmentation tool development. Besides, the majority of techniques are implemented on CT or DCE-MRI (high-contrasted images).

In this project, in order to implement a multi-class segmentation tool for kidney cortex and medulla detection and segmentation, we used T1-maps. T1-mapping images were generated from registered T1-images using non-registered groupwise method and PCA2 metric. It is also necessary

to segment the kidney as a whole. Among renal multiclass segmentation techniques intensity-based thresholding is the most simple one. It requires manually defined threshold for each T1-map. Fig. 1 depicts medulla segmentation example based on manually defined and histogram based threshold definition. Despite its simplicity and low computation time, human interaction and parameter setting is needed.

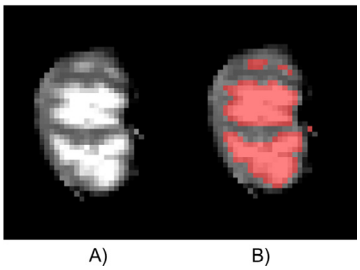

Figure 1. Example result of intensity-based thresholding of renal medulla. A) T1-Mapping image. B) Segmented medulla.

We initially discarded CNN model implementation, as it requires both cortex and medulla regions annotation. However there are different and more complex approaches that provide robust segmentation results:

- *Region Growing* methods and *Shape based* approaches with active contours.
- *Gaussian Mixture Models (GMM)* implementation, where kidney image segmentation is performed by fitting a mixture model that is a composition form of several Gaussian distributions to intensity histograms [9].

References

[1] Facts About Chronic Kidney Disease. en-US. *National Kidney Foundation.* (2021) (May 2020).

[2] Echeverria-Chasco, R. *et al.* Optimization of pseudo-continuous arterial spin labeling for renal perfusion imaging. eng. *Magnetic Resonance in Medicine* **85,** 1507-1521. ISS±: 1522-2594 (Mar. 2021).

[3] Huizinga, W *et al.* PCA-based groupwise image registration for quantitative MRI. (2021) (2016).

[4] Klein, S, Staring, M, Murphy, K, Viergever, M. A. & Pluim, J. P. W. elastix: a toolbox for intensity-based medical image registration. eng. *IEEE transactions on medical imaging* **29,** 196-205. ISS±: 1558-254X (Jan. 2010).

[5] Daniel, A. J. *et al.* Automated renal segmentation in healthy and chronic kidney disease subjects using a convolutional neural network. eng. *Magnetic Resonance in Medicine* **86,** 1125-1136. ISS±: 1522-2594 (Aug. 2021).

[6] Xiong, X & De la Torre, F. *Supervised Descent Method and Its Applications to Face Alignment* en. in *2013 IEEE Conference on Computer Vision and Pattern Recognition* (IEEE, Portland, OR, USA, June 2013), 532-539. ISB±: 978-0-7695-4989-7. http://ieeexplore.ieee.org/document/6618919/ (2021).

[7] Ronneberger, O., Fischer, P. & Brox, T. U-Net: Convolutional Networks for Biomedical Image Segmentation. *arXiv:1505.04597 [cs].* arXiv: 1505.04597. http://arxiv.org/abs/1505.04597 (2021) (May 2015).

[8] He, K., Gkioxari, G., Dollár, P. & Girshick, R. *Mask R-CNN* in *2017 IEEE International Conference on Computer Vision (ICCV)* (2017), 2980-2988.

[9] Goceri, E. Automatic Kidney Segmentation Using Gaussian Mixture Model on MRI Sequences. *Lecture Notes in Electrical Engineering* **99,** 23-29 (July 2011).

Analysis and Implementation of Wireless Communications Systems and IoT with Human Body Interference in Inhomogeneous Environments

Imanol Picallo Guembe
Electric, Electronic and Communication Engineering Dept.
Public University of Navarre
Pamplona, Spain
imanol.picallo@unavarra.es

Hicham Klaina
Electric, Electronic and Communication Engineering Dept.
Public University of Navarre
Pamplona, Spain
hicham.klaina@unavarra.es

Leyre Azpilicueta
School of Engineering and Sciences
Tecnologico de Monterrey
Monterrey, Mexico
leyre.azpilicueta@tec.mx

Ana Vazquez Alejos
Signal Theory and Communications Dept.
University of Vigo
Vigo, Spain
analejos@uvigo.es

Peio Lopez-Iturri
Electric, Electronic and Communication Engineering Dept.
Public University of Navarre
Pamplona, Spain
peio.lopez@unavarra.es

Francisco Falcone
Electric, Electronic and Communication Engineering Dept.
Public University of Navarre
Pamplona, Spain
francisco.falcone@unavarra.es

***Abstract*—The Integration of wireless communication systems is one of the main drivers of the development of the future connected society. However, this will cause challenges due to the non-static channel effect and interference impact. For this reason, a research work is proposed that enables to obtain optimal node location in relation to radio planning tasks (coverage/capacity analysis, number of lost packets, devices' consumption...), as well as to characterize the environments considering obstacles and human body being, in terms of the received power level in the complete simulation volume and at the time domain level. This will help derive wireless channel models taking into account real channel variations to deploy a Wireless Sensor Network (WSN) and reduce the impact on wireless systems performance.**

Keywords*—Internet of Things, wireless characterization, Wireless Sensor Network, 3D Ray Launching, body interference

I. Introduction

Due to the high demand for connectivity and low latency anywhere, wireless devices will grow exponentially in the coming years. Thanks to the deployment of 5G networks, the paradigm of the Internet of Things (IoT) will be promoted, which will allow meet these demands and transform society at an economic and social level. Moreover, industry digitalization will be based on Industry 4.0, enabling companies to combine advanced techniques in the fabrication and operation process together with smart technologies, thanks mainly to the Industrial Internet of Things (IIoT). Another key term that will become a reality with emerging 5G networks is the Intelligent Transport System (ITS), which allows for evolution towards full connectivity to enable services such as optimized route planning or autonomous driving within a Smart City. As a result of the high number of devices, potential interfering systems during the communication will strongly increase significantly, requiring an in-depth analysis of their behavior in complex and non-static environments due to the fact that cause the weakening of the wireless channel response.

For this reason, the research work is defined from the point of view of analyzing the behavior of the electromagnetic waves in inhomogeneous environments, that is, radio electrically complex environments that must be characterized in order to perform radio-planning tasks. In this way, the performance of the wireless communication systems will be evaluated at both the experimental and simulation level. Most of the environments, both the indoors (such as homes, auditoriums, sports venues...) and the outdoors (such as forests, cities...), depend strongly on the morphology of the scenario and the chosen location for the nodes deployment. Another critical factor to consider in this kind of environment is the presence of human beings that make dynamic scenarios and, depending on the density of people, could be a limiting factor for the devices' communication.

The most relevant propagation phenomenon in this kind of environment is the multipath effect, which is produced due to a set of phenomena such as reflection, diffraction and dispersion that affect electromagnetic waves during their propagation. For example, in vegetation surroundings, according to the vegetation density, the environment can be more diffractive (low density) or more dispersive (high density) [1]. Indoor environments, especially morphologically complex scenarios, cause an inherent difficulty on the waves propagation due to the high number of obstacles within it. In addition, the presence of humans within these environments play a key role due to the fact that the human body absorbs a significant amount of electromagnetic waves, causing the shadowing effect, which has more influence when the number of people increases, for example, in a congress center [2].

II. Methods

In order to characterize the above-mentioned environments analytically, the literature shows that techniques based on Ray Tracing are appropriate approaches for the wireless channel characterization due to the accuracy of the obtained results and the computational time required. Therefore, an in-house implemented deterministic 3D Ray Launching (3D-RL) algorithm [3] optimized with hybrid simulation has been used to analyze, characterize, and model real environments for optimal radio planning. From the point of view of the experimental analysis, a set of wireless systems from PAN (Personal Area Network) to WAN (Wide Area Network), such as ZigBee, UWB (Ultra-Wideband) and LoRaWAN, among others, have been deployed individually or in combination according to the environment and the need to cover. All of this, to convert these types of environments into context-aware scenarios (Smart Home, Smart Health, Smart Nature...), considering accuracy and optimization on the deployments of the WSN.

III. Main Results and Discussion

In this section, the main results of the research work that have been published in JCR/SJR indexed journals are presented. Fig. 1 shows the design and validation of an Augmented Reality system for impaired people in Baluarte Auditorium [2]. Fig. 2 shows a basketball player on-body biophysical parameter monitoring based on WSN integration [4]. Finally, in Fig. 3 and Table 1, a wireless characterization of an UWB-based system in an industrial environment is assessed [5].

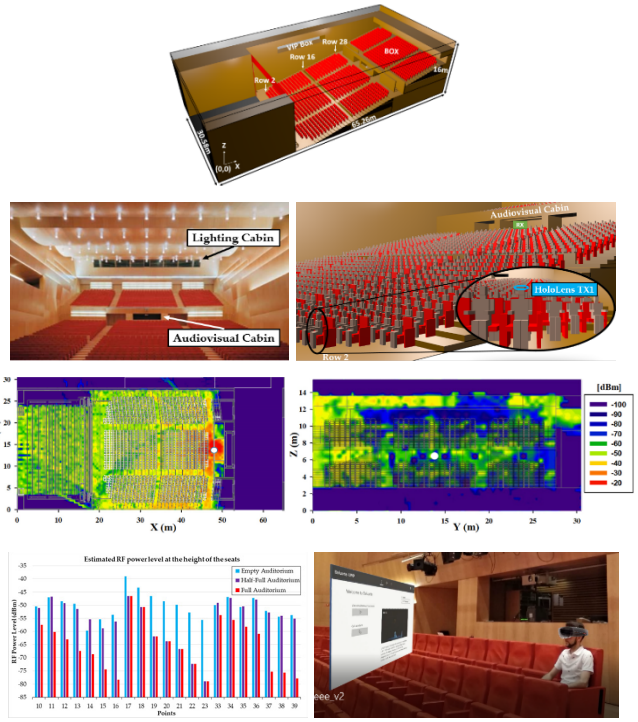

Figure 1. (a) Baluarte Palace of Congresses and Auditorium of Navarre scenario created with the 3D-RL tool; (b) Main auditorium real view; (c) Full auditorium with 1,568 people seated for simulation analysis; (d) and (e) Estimated RF power distribution 2D horizontal and vertical planes (XY and YZ); (f) Comparison of estimated RF power level for three different audience distributions (empty, half-full and full auditorium); (g) AR application for Microsoft HoloLens able to help hearing-impaired people during shows in Baluarte Auditorium has been developed and tested.

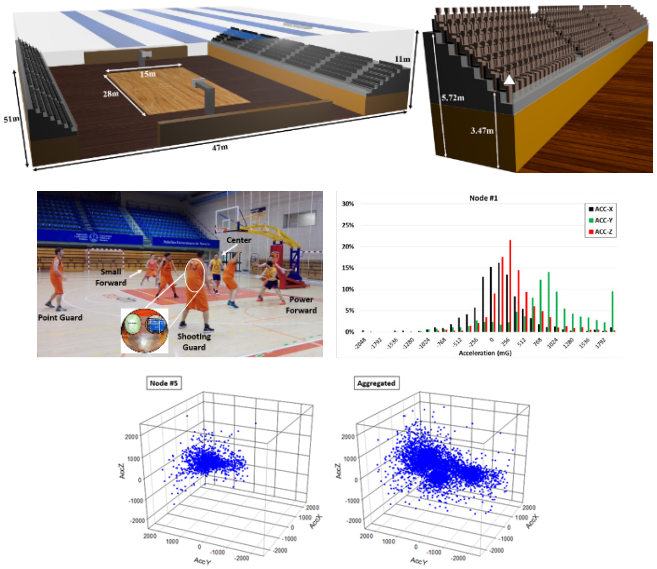

Figure 2. (a) Sport pavilion located at the Public University of Navarre created with the 3D-RL tool; (b) Detailed of a full stand including human user body models for simulation analysis; (c) Offensive tactic during the basketball training (with ZigBee node's packaging on the player's back); (d) Accelerometer data collected distribution from the Point Guard player; (e) and (f) Movement distribution from the Power Forward player and aggregated data for all the players.

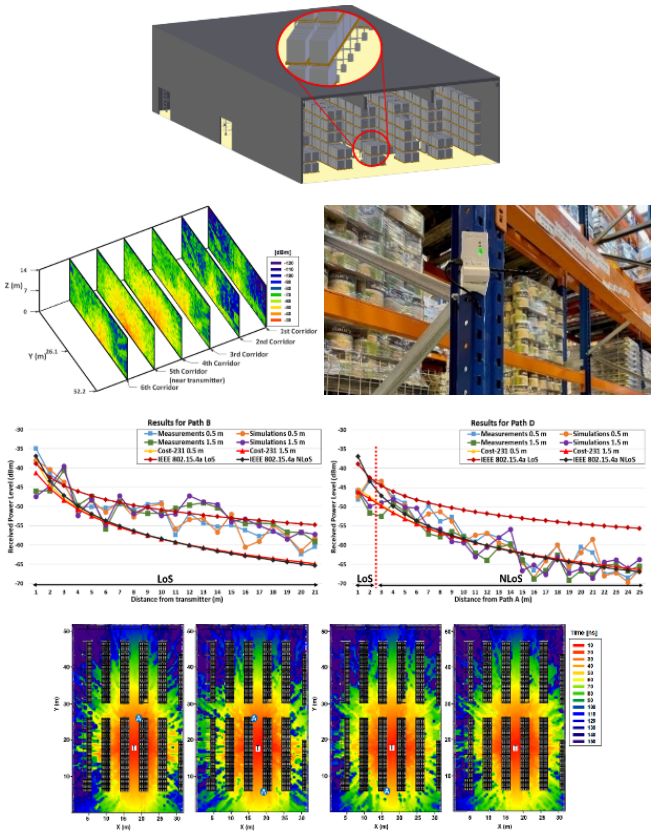

Figure 3. (a) Truck & Wheel Logistics plant created with the 3D-RL tool; (b) Estimated RF power distribution 2D vertical planes (YZ) corresponding to each corridor; (c) UWB anchor's position on the rack; (d) and (e) Comparison of the measurements, simulations with the 3D-RL tool and some empirical models for path B and D; (f) and (g) Estimated 2D ToF at the height of Anchor A20, A15, A30, A29 and Tag (T).

TABLE I. Time of Fligt (ToF) and Distance Comparison Between Tag and Anchors for Decawave (DW) Devices and 3D-RL

Anchor	*DW ToF (ns)*	*3D-RL ToF (ns)*	*DW dist. (m)*	*3D-RL dist. (m)*	*Abs. Error (cm)*
A20	27.95	24.04	8.38	7.21	**117**
A15	28.09	27.08	8.42	8.12	**30**
A29	38.98	40.13	11.69	12.04	**35**
A30	38.96	39.0	11.69	11.70	**1**

IV. Future Work

As future work, we are working on analyzing sub-and millimeter-wave through-human body and vegetation scattering effect evaluated at both the experimental and simulation levels.

References

[1] I. Picallo et al., "A Radio Channel Model for D2D Communications Blocked by Single Trees in Forest Environments," *Sensors*, vol. 19, pp. 4606, 2019.

[2] I. Picallo et al., "Design and Experimental Validation of an Augmented Reality System With Wireless Integration for Context Aware Enhanced Show Experience in Auditoriums," *IEEE Access*, vol. 9, pp. 5466-5484, 2020.

[3] L. Azpilicueta et al., "Convergence analysis in deterministic 3D ray launching radio channel estimation in complex environments," *Appl. Comput. Electromagn. Soc. J.*, vol. 29, pp. 256-271, 2014.

[4] I. Picallo et al., "Basketball Player On-Body Biophysical and Environmental Parameter Monitoring Based on Wireless Sensor Network Integration," *IEEE Access*, vol. 9, pp. 27051-27066, 2021.

[5] I. Picallo et al., "Wireless Characterization and Assessment of an UWB-Based System in Industrial Environments," *IEEE Access*, vol. 9, pp. 107824-107841, 2021.

Development and validation of an automatic and intelligent system for medullation and average diameter evaluation to Alpaca, Llama and Mohair fibers

Max Quispe Bonilla
Technological Development Laboratory
Maxcorp Technologies S.A.C
Lima, Peru
maxdavid22@gmail.com

Egdar Quispe Peña
Research laboratory
Natural Fibers Tech S.A.C
Lima, Peru
edgarquispe62@gmail.com

Luis Serrano-Arriezu, Jesús D. Trigo
Institute of Smart Cities
Public University of Navarra
Pamplona, Spain
lserrano@unavarra.es;
jesusdaniel.trigo@unavarra.es

Christian Quispe Bonilla
Data Science Laboratory
Neural X S.A.C
Lima, Peru
xtian_carlos@hotmail.com

***Abstract*—The aim of this work was to develop and validate an automatic and intelligent system (based in artificial intelligence) capable of quantify and identify fibers, by type of medullation in 5 categories. This work was carried out in Lima, Peru. To develop the software a trained model was generated based on You Only Look at Once for medullation and DenseNet for average fiber diameter (AFD), using Python. Language C was used to develop the graphical user interface. For the hardware; mechanical, electronic and optical subsystems was design and development. Samples of white alpaca, llama and mohair fibers (2108, 1858, 901 fibers, respectively) were evaluated for identification the fibers medullation. Additionally, AFD of 197 samples of white alpacas were measured with two methods. This system identifies 5 types of medullation and measures the diameter of the fibers. Each sample is evaluated in 40 sec, considering about 1500 fibers/sample. At two-proportion z-test of different fiber medullation types obtained with direct counting and our system no significant differences were found. At t-test of AFD obtained with OFDA device and our system no significant difference were found. The relationship between these methods was very stronger (r=0.95). The use of this system is recommended for fiber evaluation for the purpose of genetic improvement of fibers in animal production; purchase-sale, and processing of fiber to verify the quality of fibers; and research on medullation to increase knowledge about alpaca, llama and mohair fibers.**

***Keywords*—Alpaca, Fibers medullation, Artificial intelligence.**

I. Introduction

The reduction or elimination of strongly medullated fibers (or objectionable fibers), and continuous fibers of the mohair, alpacas and llamas, is imperative, because these fibers constitute a problem for animal production and the textile industry [1]. Therefore, it is essential to have a practical procedure for the identification and quantification of these fibers. The objective method used to measure incidence medullated fibers – Projection microscopy (PM) – is not practical because it is laborious, expensive and time consuming [2], and others methods are neither exact or precise [3]. For these reasons, the present work was carried out with the aim of developing and validating an automatic and intelligent system (based in artificial intelligence [IA]) capable of quantify and identify fibers, by type of medullation in five categories [Non medullated (NM), Fragmented medulle (FM), Uncontinuously medullated (UM), Continously medullated (CM) and Strongly medullated (SM)] and to measure average fiber diameter (AFD) of each of these categories.

II. Materials and methods

A. Location

This technological development was carried out in Lima, Peru.

B. Model development using Artificial Intelligence (AI)

To develop AI-based software (capable to identify fibers by medullation type and to measure AFD), a trained model was generated based on "You Only Look at Once" (YOLO) for medullation and DenseNet for AFD, using Python and the Pytorch framework. Programming language C ++ and C # were used to develop the graphical user interface (GUI).

C. The hardware for use of AI-based software

For hardware development, three sub systems were considered: mechanical, electronic, optical. Autodesk Inventor program was used for the design. Later, some pieces were printed in polylactic acid (PLA) and resin with 3D printers and the others mechanized in different machines. Hardware and software was called IA-Fiber Med system (IA-FiMeSy).

D. Samples preparation

Samples of white alpaca, llama and mohair fibers (2108, 1858, 901 fibers, respectively) were evaluated about identification fibers according medullation type with direct counting (DC) and IA-FiMeSy) methods. Additionally, AFD of 197 samples of white alpacas were measured with OFDA and IA-FiMeSy methods. Z-test. T-test, correlation analysis and linear regression were used to compare results obtained from medullation and AFD with IA-FiMeSy and other methods (DC and OFDA).

III. Results

The optical subsystem of IA-FiMeSy captures the sharp fiber images for later analysis; the mechanical sub system supports and covers all other parts of the system; the electronic sub system allows to automate and control the scanning process. The AI-based software identify fibers according medullation, saves the results, allow to enter sample identification data and to view AFD histograms of fibers with and without medullation.

This new system identifies automatically NM, FM, UM, CM and SM fibers of alpaca, llama and mohair. Also measures AFD global and by medullation type. In addition, it obtains the number and percentages of NM, FM, UM, CM and SM fibers (Fig. 1). Each sample is evaluated in 40 sec, considering about 1500 fibers/sample.

At two-proportion z-test of different fiber medullation types obtained with direct counting and our system no significant differences were found (Table 1). Also, at t-test of AFD obtained with OFDA and IA-FiMeSy no significant difference were found either, but the relationship between these methods was very stronger (r=0.95).

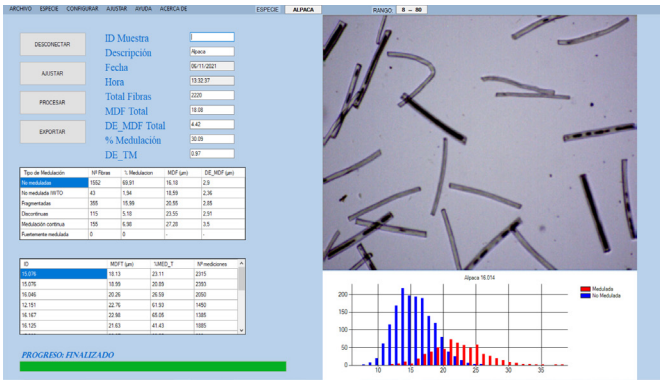

Figure 1. Graphical user interface (GUI), showing the evaluation results of fiber sample.

TABLE 1. TWO-PROPORTIONS Z-TEST RESULTS OF ALPACA, LLAMA AND MOHAIR FIBER SAMPLES ACCORDING TYPES MEDULLATION (*IN ITALIC: % WITH DIRECT COUNTING*; **IN BOLD**: % WITH IA-FIMESY; IN RED: P-VALUE)

Sample	*NM*	*FM*	*UM*	*MC*	*SM*
Alpaca: N= 2108	*25.41* **26.06** 0.698	*23.85* **24.05** 0.902	*14.53* **13.89** 0.480	*30.33* **31.59** 0.635	*2.76* **1.72** 0.069
Llama: N= 1858	*64.21* **63.38** 0.600	*16.79* **16.99** 0.874	4.63 **4.58** 0.942	*10.66* **11.31** 0.528	*1.61* **1.27** 0.380
Mohair: N= 901	*91.11* **89.99** 0.412	*0.22* **0.54** 0.274	*0.11* **0.43** 0.191	1.44 **0.75** 0.156	*7.11* **8.29** 0.345

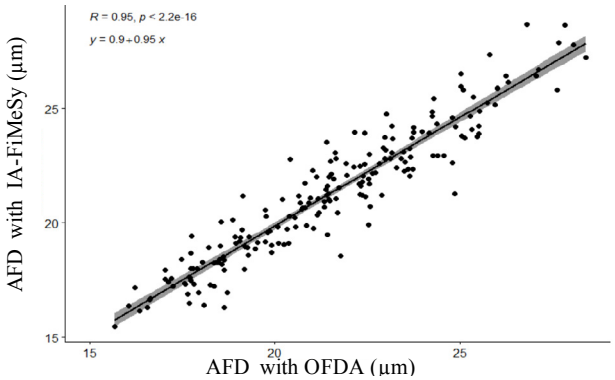

Figure 2. Scatter plot of AFD obtained with OFDA and IA-FiMeSy. Correlation Pearson and regression equation is showed, also.

IV. DISCUSSION

The fragments and medulla of the alpaca, llama and mohair fibers have the peculiar characteristics, but IA-based software identify their types medullation based in thousands of equations, so that, it was convenient to develop a model for each type of fiber. Therefore, the developed system would have the potential to evaluate the medullation of other types of fiber, for which it will be necessary to develop a model based on AI.

The similarity of the results of medullation and AFD with other commercial device (PM, and OFDA), as well as the portability, practical, no expensive, use-easy, fast are advantage of IA-FiMeSy. Therefore, it can be used in practical way by researches, farmers, marketing and others stakeholders.

With this new system a genetic improvement program can be carried out, considering as a selection criterion % of CM and SM fibers, with whose reduction – through improvement genetic in alpaca, llama and mohair fleeces – the problems of prickling, quality fabric and processing performance of these fibers would be solved [4].

V. CONCLUSION

The IA-FiMeSy is an equipment with four parts: Optical, electronical, mechanical and software, which interact to capture thousands of fibers image by means of scanning that are then processed through AI-based software to finally provide measurements of medullation and AFD. This device can be used for evaluation of alpaca, llama and mohair fibers because it has a good precision and accuracy. Additionally, fiber assessments between IA-FiMeSy with PM, PFT and OFDA have a high correlation and without significative differences. While the measurements are being carried out, the IA-FiMeSy shows sharp and defined images, allowing the user to view the images of the fibers on real time. For these considerations, the use of this new system is recommended for fiber evaluation for the purpose of genetic improvement of fibers in animal production; purchase-sale, and processing of fiber to verify the quality of fibers; and research on medullation to increase knowledge about alpaca, llama and mohair fibers.

REFERENCES

[1] L. Hunter, S Smuts, and A. Botha, "Characterizing Visually Objetionable and Non objetionable Medullated Fibers in Mohair". Journal of Natural Fibers, vol. 10: pp. 112-135, 2013.

[2] C. Lupton, and, F. Pfeiffer, "Measurement of Medullation in Wool and Mohair Using an Optical fibre Diameter Analyser". Journal of Animal Science, vol. 76: pp. 1261-1266, 1998.

[3] R. Pinares, G. Gutiérrez, A. Cruz, R. Morante, I. Cervantes, A. Burgos, and J. Gutiérrez, "Heritability of individual fiber medullation in Peruvian alpacas". Small Ruminant Research, vol. 165: pp. 93-100, August 2018.

[4] E. Frank, M. Hick, and O. Adot, "Descriptive differential attributes of type of fleeces in Llama fibre and its textile consecuence": 1. Descriptive aspects. Journal of the Textile Institute,vol. 98(3): pp. 251-259, 2007.

Micro Sized Interdigital Capacitor For Humidity Detection Based On Agarose Coating

Ignacio Vitoria
IEEC Dept.
Institute of Smart Cities, Jeronimo de Ayanz Building
Public University of Navarre
Pamplona Spain
ignacio.vitoria@unavarra.es

Dayron Armas
IEEC Dept.
Public University of Navarre
Pamplona Spain

Carlos Coronel[1], Aritz Ozcariz
IEEC Dept.
Institute of Smart Cities, Jeronimo de Ayanz Building
Public University of Navarre
Pamplona Spain

Carlos Ruiz Zamarreño
IEEC Dept.
Institute of Smart Cities, Jeronimo de Ayanz Building
Public University of Navarre
Pamplona Spain

Ignacio R. Matias
IEEC Dept.
Institute of Smart Cities, Jeronimo de Ayanz Building
Public University of Navarre
Pamplona Spain

***Abstract*—A micro sized interdigital capacitor has been proposed for the detection of relative humidity. The photolithography technique enables the fabrication of fingers with a size of 10x500 um. A thin film of agarose functionalizes the sensor for humidity sensing, which improves its performance by 155 times, obtaining a sensitivity of 32.98 pF/%RH.**

Keywords—interdigital, capacitive sensor, agarose, relative humidity

I. Introduction

Over the last few years, the interdigital capacitor sensors have gained popularity in many different fields including the internet of things and smart cities, due to its excellent performance, robustness, small size and easy readout circuit, among others [1]. Additionally, the use of flexible substrates increases the number of applications, particularly in wearable sensors [2]. Particularly, the photolithography technique has enabled the miniaturization of interdigital sensors, further improving its characteristics [3]. A wide variety of sensors, depending on its dielectric sensing material, have been researched to detect gases, temperature, contaminants etc.[4]. Among them, humidity sensors play an important role due to its importance in agricultural processes monitoring, air conditioning control, and storage supervision [5]. In this work, the fabrication and tests of humidity interdigital sensors by means of an agarose thin-film coating is presented.

II. Materials and Methods

A. Interdigital capacitor fabrication

The photolithography technique is used for the fabrication of the interdigital capacitor. It consists of various steps summarized in the Fig. 1. Firstly, the substrate of polypropylene, must be cleaned with propanol and Kimtech wipes, to remove unwanted particles. It needs to take into account that particles of dust, water or dirt can affect the final results, therefore, the entire fabrication process has to be conducted in a clean room. Next, an adhesive, Ti-Prime from the company MicroChemicals GmbH is deposited by the spin coating technique. A curing process is needed in which the substrate and the adhesive is heated to 60 ºC for 60 s. Later, the photoresist resin AZ® MIR 701 14 CP from Merck is deposited with a 100% concentration by the same technique and curing process, obtaining a yellowish color thin film (Fig. 1.1). In the next step, the PicoMaster 100-4PICO Litho BV equipment engraves the desired design of the interdigital capacitor into the resin (Fig. 1.2). The same process of curing is repeated to stabilize the modified layer. For the removal of the engraved resin, a developing procedure is needed. The AZ 400K from the company Merck is mixed in with ultrapure water in a 1:5 ratio and shaken for 1 hour. The substrate is submerged in the solution for 150 s, rinsed in ultrapure water and dried with compressed air (Fig. 1.4). Once again, the substrate is subjected to the curing process. Next, a thin film of silver is deposited to build the electrodes using the K675XD from Quorum technologies sputtering DC equipment, obtaining a thickness between 200 and 400 nm (Fig. 1.5). For the stripping process (Fig. 1.6), the resin is removed by immersing the substrate in the AZ 100 from the company Merck for 10 minutes. It is then cleaned with ultrapure soapy water for 2 minutes and then ultrapure water for an additional 2 minutes. An ultrasonic bath is used during all the stripping steps. Finally, two wires are soldered using a conductive epoxy adhesive CW2400 from Chemtronics, which are cured at 50 ºC for 10 minutes (Fig. 1.7).

B. Sensign material deposition

An agarose thin-film is deposited onto the interdigital capacitor in order to increase the sensitivity of the device to humidity variations. A solution of agarose and ultrapure water with a concentration of 1% wt/wt is prepared. The solution is heated and stirred until it reaches a temperature of 95ºC. The solution is spread by the spin coating technique and dried for 24 hours.

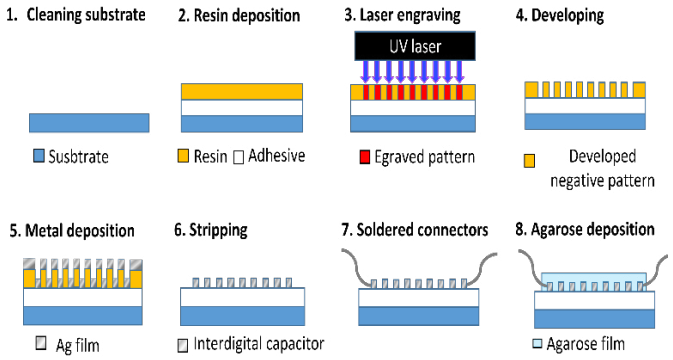

Figure 1. Summarized photolithography technique for the fabricaton of intedigital sensors.

C. Humidity test setup

Humidity is monitored by means of impedance variations of the sensor. An impedance meter E4990A from KeySight is used to measure the impedance in the range of frequencies between 100 and 100,000 Hz. The sensor is placed in a climate chamber, KMF-115 from the company Binder, to control the impedance. The capacitance of the sensor is measured at the

same time that the climate chamber changes the relative humidity in increasing steps of 10 %, from 10 % to 70% every 20 minutes. Next, relative humidity is decreased from 70 % to 10 % in steps of 20 minutes.

III. Results

The design of the interdigital capacitor consists of a matrix of 560 interdigital blocks, connected in parallel for greater capacity, with a total dimension of 270x150 mm. Each interdigital block is conformed by 16 pairs of 10 x 500 um fingers, separated by 7 µm between each other (see Fig 2.). Empty spaces of 100 µm have been added between the blocks in order to facilitate the removal of deposited metal, and thus minimize short circuits. Images of the interdigital capacitor were obtained using an optical microscope DM 2500 M from Leica using different magnification (see Fig 2), where a clear gap between the fingers preventing short circuits can be observed.

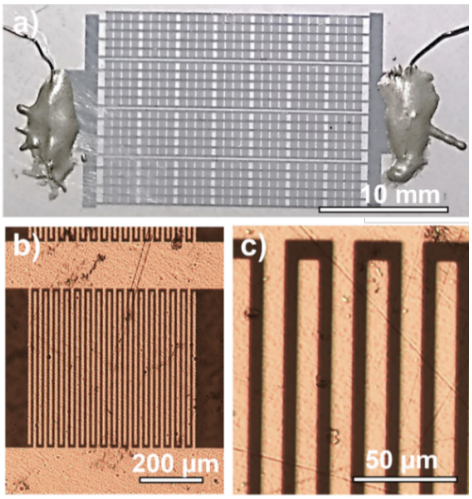

Figure 2. a) Image of the capacitor b) Close up of the interdigital block c) Close up of the fingers

Once the interdigital capacitor is fabricated, an agarose film is deposited to improve the sensitivity to humidity. In order to compare the effect of the sensing dielectric layer the sensor is tested in the climate chamber before and after the agarose deposition. The changes in the capacitance without agarose can be seen in Fig. 3. Different values of capacitance are shown with different frequencies; the lower frequencies cause the sensitivity of the sensor to be higher as a rise in the capacity was measured. In the second axis, the relative humidity of the chamber's sensors is displayed (black line) and it is observed that the sensor's response to both increasing and decreasing humidity is immediate.

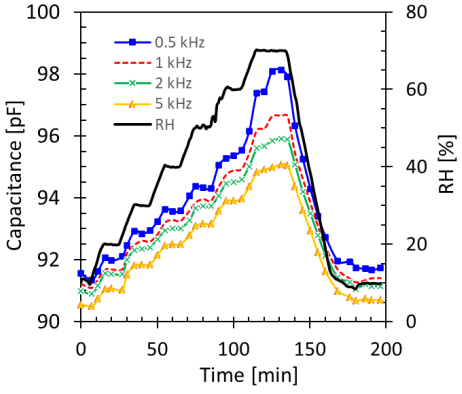

Figure 3. Capacitance at different frequencies of the interdigital (right axis) with changes of relative humidity (left axis).

The sensor is tested again with the deposition of the agarose film and the results are summarized in Fig. 4. The sensor has a linear sensitivity between 10 % and 50 %, twice than previously detected. However, between 60 % and 70 % it shows an exponential behaviour, which is increased for lower frequencies. The relative humidity sensitivity of the device with agarose, between 60-70 %, at 1 kHz is 9.5 pF/%RH (66 times larger than without agarose), and at 0.5 kHz the sensitivity of the device with agarose is 32.98 pF/%RH (155 times larger than that of the device without agarose).

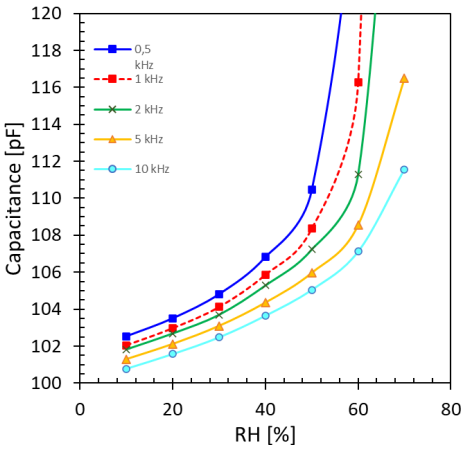

Figure 4. Capacity at different frequencies in different relative humidiy conditions of the sensor with agarose film.

IV. Conclusions

An interdigital capacitor relative humidity sensor has been proven feasible by means of the utilization of agarose thin-films. The fabrication technique implemented in this work enables the creation of small size interdigital fingers with dimensions in the order of a few micrometers. The dielectric film of agarose produces a maximum sensitivity of 32.98 pF/%RH. Improvements in the interdigital design and the use of the combination of different sensing materials in the same substrate could be implemented in future works. This study opens the door to new micro sized capacitors, where different sensitive dielectric materials could be used for a wide variety of sensors appealing for real applications on the internet of things and smart cities fields.

Acknowledgment

This research was funded by the Ministry of Science, Innovation and Universities of Spain (PRE2020-091797, PEJ2018-002958-P and PID2019-106231RB-I00) and the Institute of Smart Cities PhD Student grants.

References

[1] X. Hu and W. Yang, "Planar capacitive sensors – Designs and applications," Sens. Rev., vol. 30, no. 1, pp. 24-39, 2010.

[2] C. Gonçalves, A. F. da Silva, J. Gomes, and R. Simoes, "Wearable e-textile technologies: A review on sensors, actuators and control elements," Inventions, vol. 3, no. 1, pp. 1-13, 2018.

[3] J. C. Ferrer, J. L. Alonso, and S. F. de Ávila, "Electrical characterization of photodetectors based on poly(3-hexylthiophene-2, 5-diyl) layers," Sensors (Switzerland), vol. 14, no. 3, pp. 4484-4494, 2014.

[4] R. L. Smith, "Sensors and transducers," Eng. Handbook, Second Ed., vol. 92, no. 5, pp. 151-1-151-11, 2004.

[5] H. Farahani, R. Wagiran, and M. N. Hamidon, Humidity sensors principle, mechanism, and fabrication technologies: A comprehensive review, vol. 14, no. 5. 2014.

Autonomous robot for construction stake out

Javier I. Zaratiegui Fernández
Distributed Systems
UPNA
Pamplona, Spain
javier@cocuus.com

Carlos Juan de Dios Ursua
Robotic engineering
Cocuus System Ibérica
Cizur Menor, Spain
carlosjdd@cocuus.com

Asier Marzo Perez
Distributed Systems
UPNA
Pamplona, Spain
asier.marzo@unavarra.es

***Abstract*—Design, develop and commercial deployment of an autonomous marking device for construction stake out.**

Keywords—stake out, autonomous, stakeout,ROS, Line marker, road marker, GNSS.

I. Introduction

The stake out is the act of diving in the ground wood or metal stakes to define the bounds or limits of a construction. This job has to be done for every floor on a building construction, but is replaced with line drawings on the concrete instead of stakes. Out of these lines, the different work teams build walls, install pipes, electricity, etc., so a mistake in this stage can lead to high costs. As such, new tools have been implemented to minimize errors and optimize this task. But this tools still require qualified personnel and are subject to mistake. Therefore, we propose an autonomous device that will perform this task within <2 cm accuracy and with minimal or no human supervision. The contractor uses prefabricated elements, so the project begun with the target of open-air usage only. Later on, indoor usage was implemented and some of the elements were adapted for this new condition.

II. Technical definition

First of all, it was agreed with the contractor the functionality and performance required for the device to reach the market. Measurement precision, reliability, supported weight, minimum and maximum speed, rotation angle, IP protection for open air use, battery lasting and charging, temperature range and user interface. Secondly, the usage environment: construction sites, irregular but horizontal concrete floors, dust and material stock, used by advanced CAD software users. And last, other technical objectives were defined such as lifetime, maintenance, size range, estimated market prize, and ISO and UNE specifications. The project is called BRIT (Building Robot Intelligent Tracer).

A. Navigation

Two ublox-C099_F9P board were put on the rover to determine its relative position to a third one, the base, which obtained its global position from the Active Geodesic Navarra's Network (RGAN). The base connects to a Real Time Kinematic Positioning station (RTK) that corrects the information received from a global network of satellites (GPS, Beidu, GLONASS and Galileo) on a single station and provides up to centimeter-level accuracy. This is taken by the base station and transmitted to the rover for relative positioning. The two boards in the rover add heading information that is vital because the marking device is on one side of the device.

B. Motion

The first built device used a X-drive wheel configuration, which offers larger thrust and rotational freedom. Omni-Directional wheels with independent motors where fit to achieve 360 degree movement freedom.

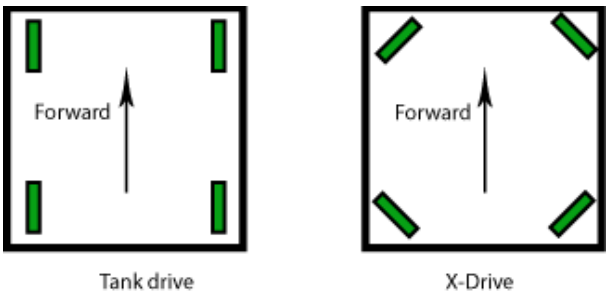

Figure 1. Tank drive versus X-Drive wheel configuration.

C. Marking

Spray systems, paint and other markers were quickly discarded. The use of diode laser engraving was tested but we finally chose a point printing system since the laser presented incompatibilities of use in the presence of people. The chosen DoD (drop on demand) system is a piezoelectric printing system, without contact, high resolution, programmable and easy to implement in our coding. Point size ranges from 0,3 to 1,4 mm.

D. Operative system

The device uses ROS (Robot Operating System) and integrates functions and algorithms in Python language to control it, take a DXF file drawing, process the different elements and boundaries and calculate a path planning strategy, obstacle avoidance, and marking strategy into g-code commands, with minimum user interaction.

E. Emergency sensors

The device has several sensors and a lidar to detect possible obstacles and avoid them. It has sensors that will perform an emergency stop to avoid falling into a hole or by the edge of the boundary. There are other sensors to control battery status and electric stability. And lastly, it will also reduce speed and/or stop in presence of people within a certain range.

F. Connectivity

The implemented boards and elements use Wi-Fi, Bluetooth and radio modules to communicate. Their performance and range and reliability in different environments has to be tested.

G. Mode of use

The workflow implies that the user exports the lines and curves he wants to draw, as well as those that define the boundary of the floor slab to be marked and, desirably, the gaps and holes to avoid so it is found a more efficient route. Units and orientation can be modified on site with the embedded touch screen but other changes require the use of a computer.

III. Results

A. Navigation system

The first tests evaluated the validity of the U-blox boards to achieve the needed relative positioning accuracy. 14 points were sampled and tests were done 28 times with different settings and satellite visibility to calibrate and adopt the best software values.

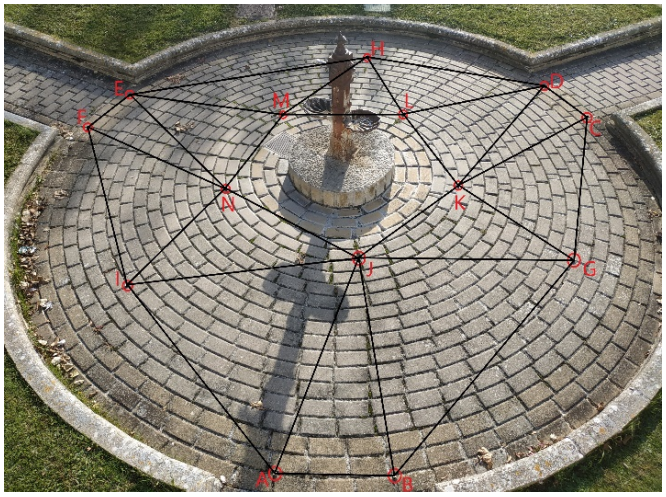

Figure 2. GNSS accuracy test point sample distribution.

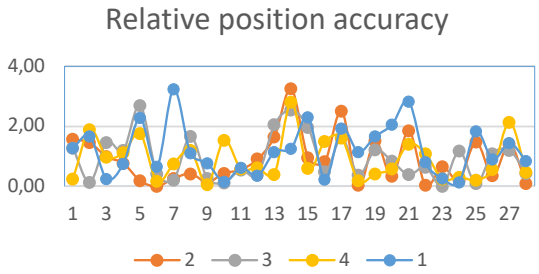

Figure 3. Accuracy test point sample distribution.

The UTM coordinates were converted to X and Y and compared to the figure drawn on the floor, and the lengths of the segments between the points were compared.

The results obtained reflect an 89,2% of sampled points remain within <2 cm and 43% within <1cm which fits and improves the range that is commonly achieved in construction sites.

B. Motion

The chosen wheels, or the quality of the first prototype, resulted in large times to reach the desired points when high accuracy mode was selected (<2cm). The results led us to change wheel type and distribution to a one axis with two wheels and one third free wheel.

• Research funded by Navarra's Government, Cocuus System Ibérica S.L. and TOPCON.

C. Version 2

The new version adopts the marking system, the operative system and the emergency system from the previous one, but included a new location system with a multi-station device, along with the new motion configuration and traction wheels.

This new location system will require qualified personnel to use the device, the multi station has to be manually moved and set, but will also be able to perform indoors, so there is a higher market potential.

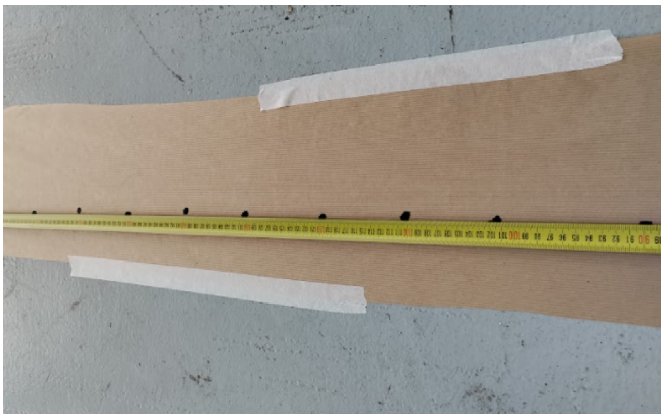

Figure 4. BRIT v2 indoor test.

IV. Objectives

The new version has to face more tests in the same and in different surfaces. Then, a construction project will be addressed and we will run the plans given by the architects. Upon success, future work will require path planning optimization and definition of the instructions to reduce the multi station allocations needed.

Acknowledgment

This paper and the research behind it would not have been possible without the exceptional support of my tutor, Asier Marzo, my supervisor, Daniel Rico, and all the personnel at Cocuus System Ibérica S.L.

References

[1] G. Ordóñez Galán, C., Rodríguez-Pérez, J. R., Martínez Torres, J., García Nieto, P.J., Analysisof the influence of forest environments on the accuracy of GPS measurements by using genetic algorithms. Mathematical and Computer Modelling, no. 54, pp. 1829-1834. ISSN:0895-71771955, 2011.

[2] J. Odolinski R, Teunissen P. Low-cost, 4-system, precise GNSS positioning: A GPS, Galileo, BDS and QZSS ionosphere-weighted RTK analysis. Measurement Science and Technology, 28(12), 2017.

[3] Zou, H., Jin, M., Jiang, H., Xie, L., & Spanos, C. J. WinIPS: WiFi-based non-intrusive indoor positioning system with online radio map construction and adaptation. IEEE Transactions on Wireless Communications, 16 (12), 8118-8130, 2017.

[4] .Qi, J., & Liu, G. P. A robust high-accuracy ultrasound indoor positioning system based on a wireless sensor network. Sensors, 17 (11), 2554, 2017.

[5] Savnani, P. S., Sisodia, H. S., Tak, D., & Mecwan, A. (2020, February). Modelling, Design and Control of a Four wheel Holonomic Drive. 7th International Conference on Signal Processing and Integrated Networks (SPIN) (pp. 879-884). IEEE, 2020.

[6] Suarez, J. D., & Correa, A. C. Design of a holonomic robotic system for interior reconstruction using SLAM. Congreso Internacional de Innovación y Tendencias en Ingeniería (CONIITI) (pp. 1-5). IEEE, 2020.